To the Graduate Council:

I am submitting herewith a thesis written by Ling Li entitled "A study of *Cyfip1* gene at the *l7Rl1* locus in mouse chromosome 7." I have examined the final electronic copy of this thesis for form and content and recommend it be accepted in partial fulfillment of the requirements for the degree of Master of Science, with a major in Life Science.

Dabney K. Johnson
Major Professor

We have read this thesis and
recommend its acceptance:

Brynn H. Voy

Naima Moustaid-Moussa

Accepted for the Council:

Carolyn R. Hodges

Vice Provost and Dean of the

Graduate School

(Original Signatures are on file with official student records)

A STUDY OF *CYFIP1* GENE AT THE *l7Rl1* LOCUS IN MOUSE CHROMOSOME 7

A Thesis Presented
for the Master of Science
Degree

The University of Tennessee, Knoxville

Ling Li
May 2007

ACKNOWLEDGEMENTS

It is my fortune that I have met so many great people in the journey of reaching this degree. The encouragement and support of these people has made possible the realization of my dream.

I would like to thank my major professor, Dr. Dabney Johnson. She provided me with strength, support and direction. I would also like to thank Dr. Yun You for the opportunity he gave to me to work in his lab. In the post several years, Yun's influence and guidance have permeated my life and instilled me how to face the challenge and conquer difficulties. He showed me how to work efficiently in being a scientist.

The thesis committee members made it possible for me to go smoothly in my project. I would like to thank Dr. Naima Moustaid-Moussa and Dr. Brynn Voy for being interested in my ideas and for being there for me whenever help is needed.

Finally, I would like to thank all the former members in Yun's lab. I would like to thank Dr. Wallace Chick, who taught me a lot in the lab and provided valuable ideas. Special thanks to Sarah Mentzer, a super-technician, who has been a great helper for me throughout the time in the lab on everything.

ABSTRACT

The large-scale mouse mutagenesis experiments conducted at Oak Ridge National Laboratory using mouse specific-locus test (SLT) have generated numerous radiation- or ENU-induced mutations. A series of mutations were mapped near the *p* gene, one of the seven marker loci in mouse chromosome 7. Complementation analyses with a panel of *p* deletions have defined a number of "functional units", among which is *l7Rl1*, a ~300kb region corresponding to human chromosome 11p14-p15 and containing four genes (from centromere to telomere): *tubulin gamma associated protein 5 (Tubgcp5), Cytoplasmic fragile X mental retardation syndrome 1 homolog (FMR1) interacting protein 1 (Cyfip1), non-imprinted in Prader-willi/angelman syndrome 2 (Nipa2), and non-imprinted in Prader-willi/angelman syndrome 1 (Nipa1)*. *l7Rl1* is known to be required for peri-implantation survival, but it has been unclear how any one of the deleted genes contributes, if at all, to the implantation failure. In this study, we continued the study of the *l7Rl1* by exploiting the DNA sequence and mutation resources available for this region of the mouse genome. *Cyfip1* is the first candidate gene among the four to cause the peri-implantation lethal phenotype. To study the function of *Cyfip1*, $Cyfip1^{Gt}/+$ transgenic mice were generated using a gene-trap ES cell line from the BayGenomics gene-trap ES cell library. However, $Cyfip1^{Gt/Gt}$ homozygotes do not show peri-implantation lethality. Instead, the $Cyfip1^{Gt/Gt}$ homozygous embryos are able to survive through the peri-implantation stage (E4.5-E6.5) and develop normally until E8.5, after which the embryonic development is arrested with defects in the central nervous system. Two N-ethyl-N-nitrosourea (ENU)-induced lethal mutation stocks, $l7Rl1^{ENU2R}$ and

l7Rl1^{ENU3R} have been previously mapped within the *l71Rl* critical interval. We performed intra- and inter-crosses for these two ENU-induced mutations as well as allelism tests with *Cyfip1*$^{Gt/+}$ mice. We have identified the two ENU mutations at the molecular level and confirmed that they are alleles of *Cyfip1*. The results suggest that *Cyfip1* plays an indispensable role in mouse embryonic development. Therefore, if the *l7Rl1* is a single-gene defect, *Cyfip1* is an unlikely candidate. However, it may still be a contributor to the *l7Rl1* lethal phenotype if the peri-implantation lethality is due to the combinatorial effects of several gene deficiencies.

TABLE OF CONTENTS

Chapter **Page**

LIST OF TABLES

Table **Page**

LIST OF FIGURES

CHAPTER I
INTRODUCTION

The fact that mouse has similar developmental, physiological, biochemical and behavioral patterns to humans, together with its high similarities to human at the genotypic level, makes it an exceptional model system to understand the human genome. The *l7Rl1* functional unit in the *p* region of mouse chromosome 7 has been defined as a peri-implantation lethal locus by complementation analysis with a panel of *p* deletions generated in Oak Ridge National Laboratory. Previous characterization of the genomic region indicated that the *l71Rl* interval contains 4 genes. But it has been unclear how any one of the deleted genes contributes, if at all, to the implantation failure. The purposes of this work are to further study the functional unit *l7Rl1* by identifying the gene responsible for the peri-implantation lethality, and to gain understanding of gene(s) involved in early embryonic development in the mouse.

The origin of the *p*-locus deletion mutations

More than half century ago, large-scale mouse mutagenesis experiments were begun in Oak Ridge National Laboratory (ORNL). Various radiation types, doses or chemical substances were extensively used as agents of mutagenesis to induce heritable mutations. These point mutations or deletion mutations provided valuable reagents for gene and function research. To understand the genotype of generated mutations and assess the average rates of induced mutations at 7 selected loci in the mouse genome, the Specific Locus Test (SLT) was designed for genetic analysis (Russell 1951). The loci

chosen to be followed in the SLT were recessive mutations with visible homozygous phenotypes that were easily distinguished and isolated from each other, and had no effect on viability or fertility. The seven loci are *a* (non-agouti, chromosome 2), *b* (brown, chromosome 4), c^{ch} (chinchilla at albino, chromosome 7), *p* (pink-eyed dilution, chromosome 7), *d* (dilute, chromosome 9), *s* (piebald-spotting, chromosome 4), and *se* (short-ear, chromosome 9). In order to perform SLT, the *T* (tests) stock mouse homozygous for all seven recessive marker loci was created for simultaneously following the genetics of seven traits (Russell 1989). The SLT was carried out by crossing *T*-stock females to the wild-type males or the wild-type males that have been previously treated with various doses of radiations or chemicals. In the absence of any mutations from the treated males, the progeny would appear wild-type. However, if a mutation has been induced at any one of the specific loci, the associated mutant phenotype will be uncovered. The test is very efficient since it only requires a single generation of breeding and visual examination. Numerous radiation- or chemically induced mutations involving each of seven marker loci have been generated in ORNL.

The pink-eyed dilution locus (*p*), one of the seven specific loci, has been identified in both mouse and human (Gardner, Nakatsu et al. 1992; Rinchik, Bultman et al. 1993) The gene encodes an integral membrane transporter protein possibly involved in transport of tyrosine (Rinchik, Bultman et al. 1993; Lee, Nicholls et al. 1994; Spritz 1994). Mutations in *p* are associated with melanin reduction in the skin, hair, and eyes and are easily scored (Rinchik, Bultman et al. 1993; Gardner, Nakatsu et al. 1992; Russell 1951; Spritz 1994). For example, in the SLT of the *p* locus, heterozygous G1 progeny carrying a *p*-locus mutation (p^{*}/p), where p^{*} represents a new recessive mutation,

has pink eye pigmentation instead of wild-type eye pigmentation (Russell, Montgomery et al. 1995). A large number of *p*-locus mutations have been recovered over many years at ORNL. Among those mutations, most are radiation-induced deletion mutants, which at least part of the *p* gene as well as various lengths of chromosome segments immediately surrounding the *p* locus are deleted (Russell, Montgomery et al. 1995). The identified *p*-locus mutation were recovered as p^* +/*p* c^{ch}, where p^* represents any new *p*-locus mutation, and c^{ch}, chinchilla, is an allele at the *albino* locus which is 14cM distal to the *p*-locus. The breeding protocol used to generate founder lines for the propagation of each new mutation is described below: the primary mutant was mated to + c^{ch}/+ c^{ch}. At least 6 wild-type offspring were collected as the founder of a line. Each founder was again cross to + c^{ch}/+ c^{ch} and wild-type offspring tested to carry p^* (or *p* in 14% of the line) were then backcrossed to the founder. Lines that failed to yield pink-eyed or intermediate phenotype progeny were assumed to carry a prenatally lethal mutation involving *p*, and such mutations were subsequently propagated from the one of the founder lines (Russell, Montgomery et al. 1995).

Complementation and deletion analyses of the *p*- deletion mutations

To characterize the genomic structure of surrounding region of *p* locus, large-scale complementation and deletion analyses of 45 *p*-deletion mutations were performed. The phenotypes of these mutations were characterized in terms of pigmentation, neuro-motor behavior, viability, and fitness (Russell, Montgomery et al. 1995).

All 45 mutations in the study were homozygous lethal prenatally, neonatally, or postnatally (Russell, Montgomery et al. 1995). Based on the phenotype, these

independent mutations were categorized into six groups when in combination with the standard *p* allele: 38 mutations produce hair and eye pigmentation indistinguishable from *p/p*, among which, 33 are prenatally lethal in homozygotes (generically designated p^{pl}), 4 are neonatally lethal (p^{nl}), and one is juvenile lethal (p^{jl}). Another five mutations, designated p^{x}, produce pigmentation that is intermediate between *p/p* and wild-type, among which two are prenatally lethal in homozygotes (p^{xpl}); and the other three are juvenile lethal (p^{xjl}). Finally, two mutations produce a mottled pigmentation pattern; and homozygotes of both mutations were classified as juvenile lethal, with the generic designation p^{mjl} (Russell, Montgomery et al. 1995).

For the complementation analyses, 810 combinations of crosses of two different *p* mutations were made. The preferred cross was between + c^{ch}/p^{1} + and + c^{ch}/p^{2} +, where p^{1} and p^{2} represent any two different p-locus mutations. If no p^{1}/p^{2} offspring were observed, the combination of *p* mutations was characterized as prenatally lethal. Compound heterozygotes that survived to or past birth was classified into four categories: neonatal lethal (*nl*); severe juvenile lethal (*jls*); mild juvenile lethal (*jlm*); and viable (*v*) (Russell, Montgomery et al. 1995).

Based on the complementation analysis between different lethal phenotype mutations, several functional units in the p-region of mouse chromosome 7 were identified. Each represents a specific deletion phenotype and is located within an interval bounded by individual deletion breakpoints. The generated complementation map pointed out prenatal lethal 1 (*pl-1)* and neonatal lethal (*nl)* functional units located on opposite sides of *p*, proximal and distal to *p* respectively. Also, the juvenile lethal unit *jl* lies between *pl-1* and *p* (Russell, Montgomery et al. 1995).

Molecular analysis of the *p*-locus deletions

To expand the resolution of the *p*-deletion map, a molecular map was also generated for the *p*-locus region. Seventeen different molecular probes were applied to examine deletions or rearrangements in the *p*-deletion mutations for the construction of a map overlapping among deletions. Recombination distances between loci were estimated through mapping to the Oak Ridge Interspecific Backcross panel (Johnson, Stubbs et al. 1995). The map provided more detailed information for cloning and characterizing genes correlated with specific deletion phenotypes. For example, genes responsible for two of the functional units, *nl* and *jl* have been identified. Neonatally lethal mutations showed a phenotype of cleft palate disorder in the homozygotes. By genetic and molecular analysis of a number of the *p*-deletion mutations, the α_5 and ß$_3$ subunit of the type A γ-aminobutyric acid receptor (*Gabra5* and *Gabrb3*, respectively) were discovered in the functional unit *nl;* and *Gabrb3* was proven to be the gene responsible to the cleft palate in *nl* mutants (Culiat, Stubbs et al. 1993; Culiat, Stubbs et al. 1994) Furthermore, 3 non-complementing ENU-induced mutations were mapped to the critical region of the *jl* functional unit, which allowed identification of a single gene whose dysfunction results in the juvenile lethality. The gene was further cloned and identified as *Hect domain and RLD2* (*Hect2*) (Rinchik, Carpenter et al. 1995; Ji, Walkowicz et al. 1999)

The *pl-1* function unit has been defined as a chromosome region proximal to *p*-locus, and bounded by the proximal breakpoints of 19 deletions and the proximal breakpoints of other 4 deletions. The locus associated with the *pl-1* functional unit was designated *l7Rl1* (Russell, Montgomery et al. 1995). Homozygous deletion of *l7Rl1* results in prenatal lethality. $p^{226THO\text{-}I}/p^{x}$ heterozygotes were intercrossed, $p^{226THO\text{-}I}$ is a

deletion known of affect *l7Rl1*, and p^x is a radiation-induced viable allele of *p* locus. Uteri dissection at embryonic day (E) 14.5 showed homozygous embryos degenerated, only resorption moles can be observed, suggesting homozygous mutants died at the early post-implantation stage(Wu, Rinchik et al. 2000).

Mapping the minimum critical region for *l7Rl1* locus

Previous genetic and molecular analysis indicated that *l7Rl1* is located between the growth arrest-2 gene *(Gas2)* and *p* in mouse chromosome 7, a distance of approximately 2.2cM (Johnson, Stubbs et al. 1995). To further dissect the critical region of *l7Rl1* and identify the gene(s) harbored in this region, an integrated deletion/physical map of this region has been constructed for genetic analysis (Wu, Rinchik et al. 2000).

First, three microsatellite markers, *D7Mit86*, *D7Mit70*, and *D7Mit295* were mapped to the *l7Rl1* critical region by PCR analysis using mit-specific primers and interspecific hybrid DNAs of *Mus musculus/M. spretus* or *M. musculus/M. castaneous*, with the *M. musculus* chromosome containing a *p* deletion. Second, the *leucine zipper protein 2* gene (*Luzp2*), a gene cloned from the proximal deletion breakpoint of one of the *l7Rl1* mutation, was excluded from *l7Rl1* by the facts that *Luzp2* is intact in three *l7Rl1* deletions and $Luzp2^{-}/Luzp2^{-}$ knockout mice are viable(Wu, Rinchik et al. 2000). To start to construct the physical map between *Luzp2* and *p*, on the proximal and distal end, primers designed from the 5' end of the *Luzp2* cDNA and *D7Mit70* primers were used to screen a mouse YAC genomic library, respectively. End clone from positive YACs were further used to screen for BACs and YACs to extend coverage of the physical contig. Restriction fragment length variant (RFLV) analysis, a genetic polymorphism analysis

with respect to the observed length of a restriction fragment, was used to map those end clones to the *p*-deletion complex and the insert sizes of the genomic clones were determined. After several rounds of screening and mapping of BACs and YACs, the physical map was completed after linking the distal and proximal groups of the contig (Wu, Rinchik et al. 2000).

The physical map further defined the proximal breakpoints of nineteen *l7Rl1* deletion mutations, and further narrowing down the critical region of *l7Rl1* was carried out by analysis of those nineteen mutations (Wu, Rinchik et al. 2000). The missing region of the smallest *l7Rl1* deletion mutation $p^{12R30Lb}$ including p^{6H}. However, p^{6H} homozygotes die as juveniles due to the deletion of the *Herc2* gene (Rinchik, Carpenter et al. 1995) and the *l71Rl* gene(s) remains intact. Thus, the minimum critical region for *l7Rl1* is between the proximal breakpoints of $p^{12R30Lb}$ and p^{6H}, which covers the 5' end of *Herc2*. Since studies have shown that *Herc2* mutation result in juvenile lethality (Johnson, Stubbs et al. 1995; Rinchik, Carpenter et al. 1995; Walkowicz, Ji et al. 1999) which is significantly different from the prenatal lethality seen in *l7Rl1* mutations, the minimum critical interval for *l7Rl1* should be between the 5' end of *Herc2* and the proximal breakpoint of $p^{12R30Lb}$. Three BAC clones, BAC G430K16, G319F6, and G306G15 cover the *l7Rl1* region, in which the combined size of G430K16 and G319F6 (300kb) covers the whole region of *l7Rl1*, and G306G15 (80kb) covers only partially (Figure 1.1) (Wu, Rinchik et al. 2000).

Figure 1.1 Mapping the minimum critical region for *l7Rl1* locus – a integrated deletion/physical map of the chromosome segment surrounding *l7Rl1* (modified from Wu 2000)

The black line in the middle represents the chromosome segment from *ru2* to *p* in mouse chromosome 7. The centromere is at the left of the chromosome. Molecular markers are listed on the chromosome line. The open boxes above the chromosome line represent chromosome segments deleted in the corresponding mutations. Lines below the chromosome line represent the individual BAC clones. The filled box above the chromosome line represents the minimum critical intervals for the *l7Rl1* functional unit.

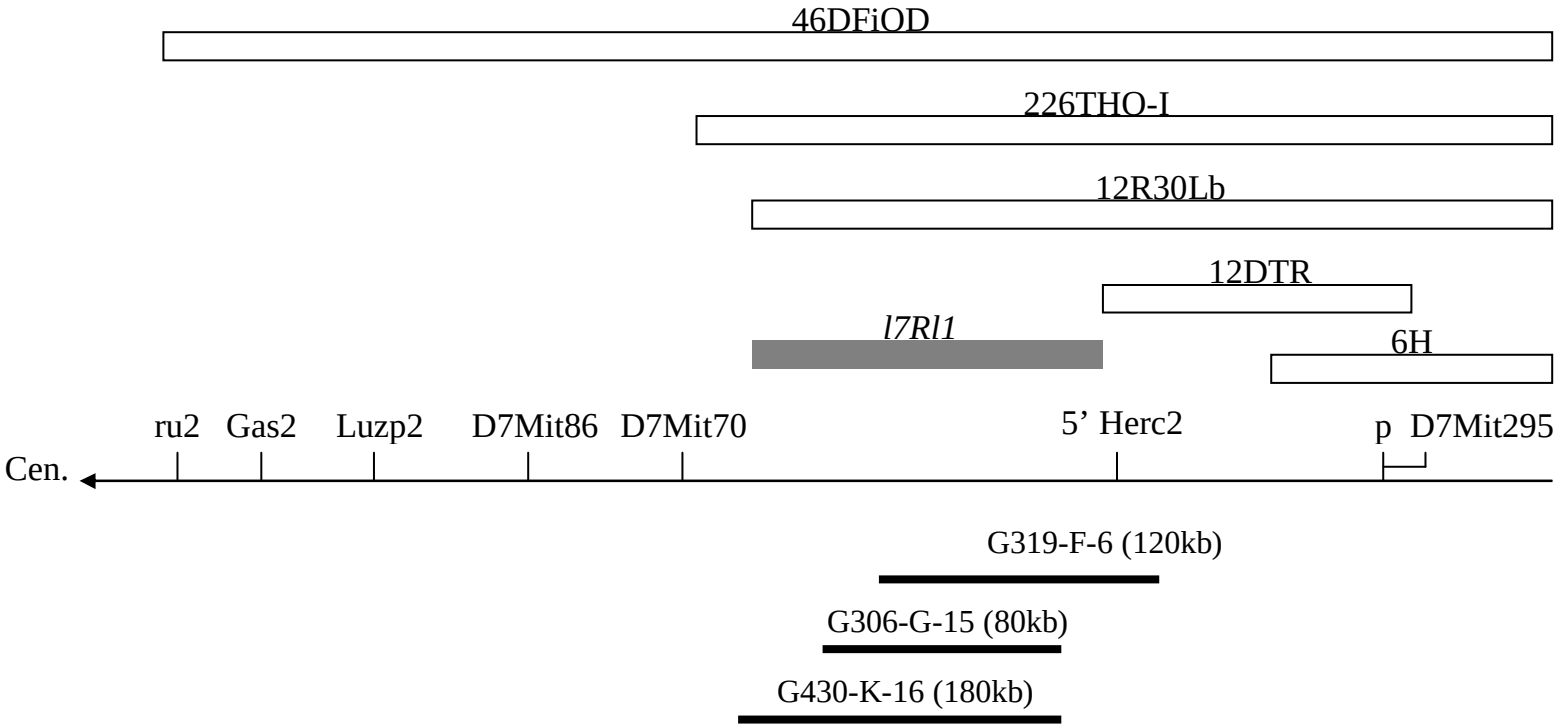
46DFiOD
226THO-I
12R30Lb
12DTR
l7Rl1
6H
ru2
Gas2
Luzp2
D7Mit86
D7Mit70
5’ Herc2
p
D7Mit295
Cen.
G319-F-6 (120kb)
G306-G-15 (80kb)
G430-K-16 (180kb)

Peri-implantation lethality of *l7Rl1* mutations

Complementation analyses have shown that homozygous deletion of *l7Rl1* results in prenatal lethality (Russell, Montgomery et al. 1995). To determine embryonic stage of developmental abnormality in *l7Rl1* mutants, heterozygous $p^{226THO\text{-}I}/p^{x}$ mice were intercrossed and cross sections of uterine swellings at E5.5 were compared with a control group. 23.1% of the decidua from the experimental mating contained degenerating embryos, whereas only 4.9% degenerating embryos were observed in the control mating. Statistically, this is a strong evidence that the excess abnormal embryos observed in the experimental mating are $p^{226THO\text{-}I}/\ p^{226THO\text{-}I}$ homozygotes. Furthermore, histological studies of the cross sections of those uterine swellings at E5.5 have been performed. The result demonstrated that normal embryos elongate into an egg-cylinder structure with differentiated embryonic and extraembryonic ectoderm; however, presumptive $p^{226THO\text{-}I}/\ p^{226THO\text{-}I}$ mutant embryos show that although mutant embryos are able to attach to the uterine epithelium and induce the decidual response, no egg-cylinder structure have been formed and mutant embryos undergo degeneration (Figure 1.2) (Wu, Rinchik et al. 2000). The result suggests that *l7Rl1* is required for peri-implantation survival in the mouse.

Identification of two mutations within the *l7Rl1* locus by ENU saturation mutagenesis

N-ethyl-*N*-nitrosourea (ENU) is a wildly used supermutagen in mice and is known to induce primarily point mutations in spermatogonial stem cells (Popp, Bailiff et al. 1983; Brannan, Bedell et al. 1992; Zdarsky, Favor et al. 1990). *Ruby eye* 2 (*ru*2), a

Figure 1. 2 Histological sections of a normal (A) and two presumptive $^{p226THO-I}$ / $^{p226THO-I}$ mutant embryos (B, C) at E5.5 (Wu M. et al., 2000).

eee, extraembryonic ectoderm; ee, embryonic ectoderm; pe, parietal endoderm; ve, visceral endoderm; pac, proamniotic cavity; Rm, Reichert's membrane; mt, mural trophectoderm; em, embryo. (A) wild-type embryo has elongated into an egg-cylinder structure with differentiated embryonic and extraembryonic ectoderm. (B, C) presumptive $^{p226THO-I}$/ $^{p226THO-I}$ mutant embryos were able to attach to the uterine epithelium and induce the decidual response, but no egg-cylinder has formed at E5.5. Darkly stained pyknotic cells have accumulated in the positive of the indiscernible embryo proper, indicating the embryo undergoing degeneration.

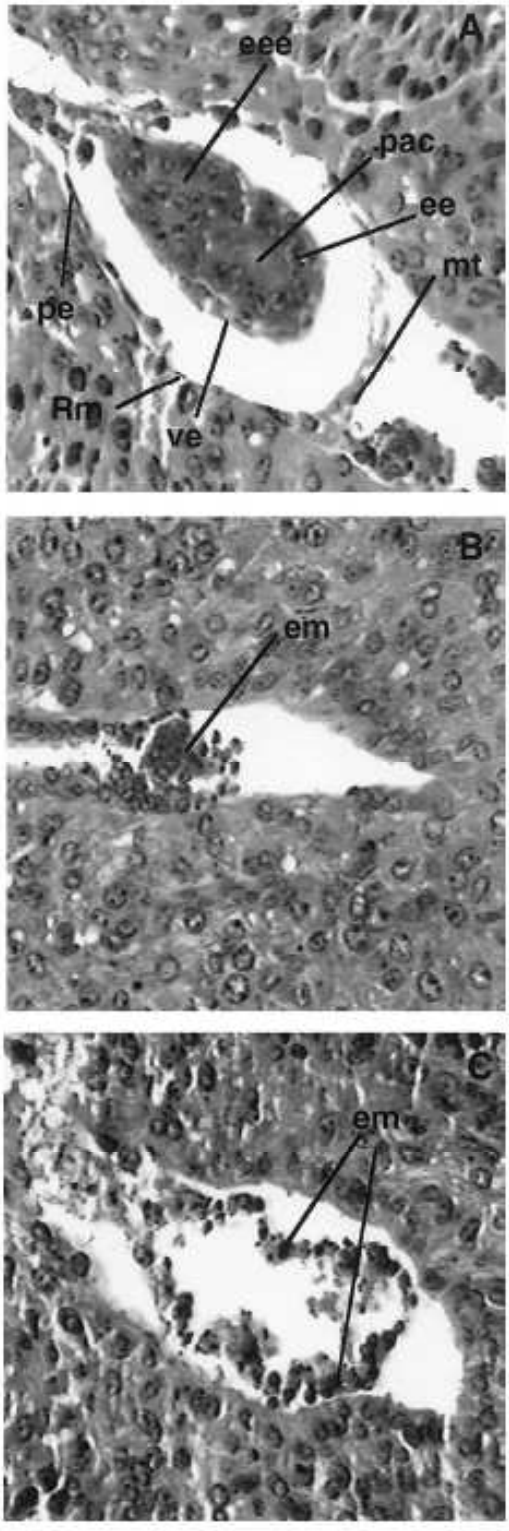
A
eee
pac
ee
mt
pe
Rm
ve
B
em
C
em

coat-color marker that maps ~3 cM proximal to *p* (Eicher 1970) has been used as a standard marker in the deletion mapping for the *p* mutations. $p^{46DFiOD}$ was the only mutation in which the *ru2* locus was found to be deleted (Johnson, Stubbs et al. 1995). In order to use the *p*-deletion mutations to recover ENU induced point mutations, male r*u2 p/ru2 p* mice were mutagenized with ENU and were mated to wild-type (C57BL/10R1 x C3Hf/R1) F1 females. All G_1 females from this cross were then crossed to $p^x/p^{46DFiOD}$ mice. Only ruby-eyed and pink-eyed G_2 offspring, carrying the mutagenized chromosome opposite the deletion in $p^{46DFiOD}$ should manifest any new phenotypes caused by the newly induced recessive mutations. An absence of pink-eyed dilute, ruby animals in a particular pedigree indicated that the newly induced ENU mutation was lethal (Figure 1.3) (Rinchik, Carpenter et al. 1995). As we mentioned previously in this introduction, 3 noncomplementing ENU-induced mutations recovered in this study were utilized in identifying the single gene, *Herc2*, whose dysfunction results in the juvenile lethality (Rinchik, Carpenter et al. 1995).

Two independent, recessive-lethal mutations were found to be segregating in the 785DSJ and 828DSJ pedigrees. The two ENU-induced lethal mutations were then fine-mapped on the large panel of *p*-deletion complex maintained at ORNL (Rinchik, Carpenter et al. 2002). Female p^x/p^{Del} deletion heterozygotes were crossed to *m p/+* p^x males that were first proved by progeny test to be heterozygous for each ENU-induced mutation. If *m* maps outside of a particular p^{Del}, then 25% of the offspring should be pink-eyed *m p/+* p^{Del}. However, if *m* maps within a particular p^{Del}, then the pink-eyed dilute animals will be absent (Rinchik, Carpenter et al. 2002; Rinchik, Carpenter et al. 1995). Deletion mapping of the 785DSJ and 828DSJ prenatal-lethal mutations by this

Figure 1.3 Breeding protocol used to recover ENU-induced recessive mutations mapping within the $p^{46DFiOD}$ deletion (Rinchik 2002)

ru2, ruby-eye 2; p, pink-eyed dilution; *m* indicates an ENU-induced point mutation near the *p* gene. In the G_0 generation, male mice which had been treated with ENU were mated with wild type F_1 females. G_1 females were then crossed to *ru2* +/ $p^{46DFiOD}$ males. Three phenotype classes were expected in the G_2 progeny: wild-type, ruby, and ruby, pink-eyed dilute. The ruby pink-eyed dilute class highlights with the heavily outlined box was the test class for mutations. The lightly outlined box highlights the ruby class, which can be used to recover and propagate the mutations.

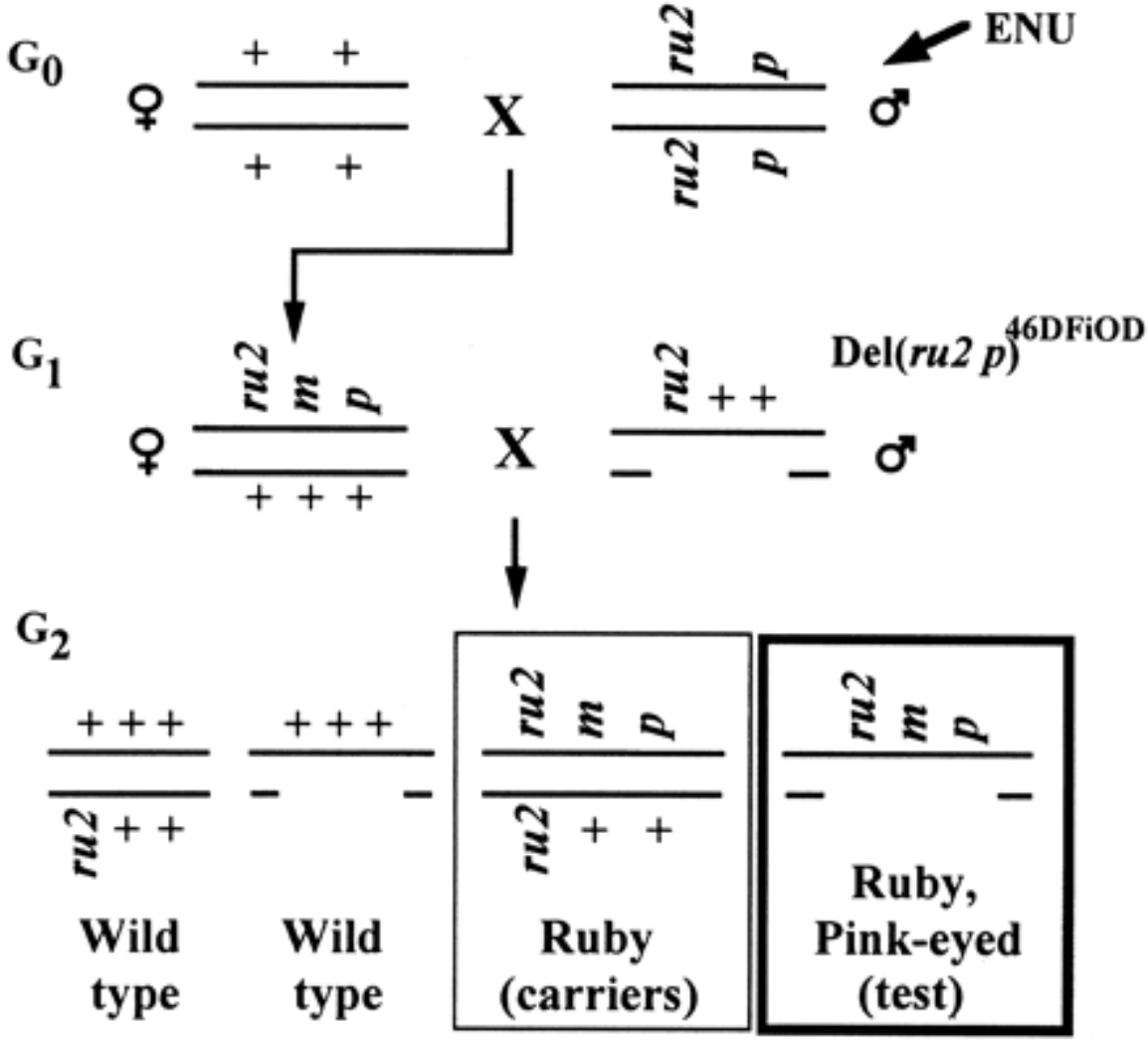
G0
+ +
♀
X
ru2 p
ru2 p
♂
ENU
G1
ru2 m p
+ + +
♀
X
ru2 + +
– –
♂
Del(ru2 p)46DFiOD
G2
+ + +
ru2 + +
Wild type
+ + +
– –
Wild type
ru2 m p
ru2 + +
Ruby (carriers)
ru2 m p
– –
Ruby, Pink-eyed (test)

approach revealed that they both mapped within the $p^{12R30Lb}$ deletion but outside of p^{6H} deletion. This region contains *Herc2*. Further mapping using *Herc2* deletion p^{12DTR}, a small interstitial deletion of *Herc2* genomic region, ruled out the *Herc2* region. Thus, both 785DSJ and 828DSJ were mapped to the critical region of *l7Rl1*.

Genes mapped within the *l7Rl1* interval

It has been characterized by both genetic and molecular approaches that the region of mouse chromosome 7 surrounding the *p* locus shares homology with human genomic regions 15q11-q13 and 11p14-p15 (Rinchik, Carpenter et al. 1995; Nicholls, Gottlieb et al. 1993; Rinchik, Bultman et al. 1993; Johnson, Stubbs et al. 1995; Russell, Montgomery et al. 1995). Studies have also been shown that deletion of human chromosome 15q11-q13 is the most common reason for imprinted genetic disorders: Prader-Willi syndrome (PWS) and Angelman Syndrome (AS) (Nicholls and Knepper 2001). Molecularly, there are two common classes of deletions in patients with PWS/AS, one from breakpoint (BP) 1 to BP3 and the other from BP2 to BP3 (Knoll, Nicholls et al. 1990; Amos-Landgraf, Ji et al. 1999). PWS arises from the functional loss of a set of paternally expressed genes, whereas AS is associated with the loss of maternally express genes. Not all genes located in the human and mouse PWS/AS regions are imprinted. Four highly conserved genes were mapped between BP1 and BP2 in 15q11.2, and the non- imprinting status of these genes were identified in human and mouse (Nicholls and Knepper 2001; Chai, Locke et al. 2003). These genes are in the same respective order in human and mouse, but lie in opposite centromere-telomere orientations; these genes are *Gcp5* (γ-tubulin complex proteins 5*)*, *Cyfip1* (cytoplasmic FMR1 interacting protein 1*)*,

Nipa2 (nonimprinted in Prader-Willi/Angelman syndrome 2) and *Nipa1* (nonimprinted in Prader-Willi/Angelman syndrome 1) in the order from centromere to telomere in mouse chromosome 7 (Figure 1.4). Furthermore, these genes are located distal to *Luzp2* and proximal to Herc2 in the mouse genome, thus falling into the minimum critical region of *l7Rl1* (Chai, Locke et al. 2003).

Gcp5 belongs to a novel protein superfamily. There are six members of GCP family in the human and mouse genomes. All of these members are the components of the γ- tubulin multiprotein complex which is required for microtubule nucleation at the centrosome (Oegema, Wiese et al. 1999). Gcp5 is a newly identified member of this complex and has been found localizing to the centrosome and associating with microtubules (Murphy, Preble et al. 2001).

Both *Nipa1* and *Nipa2* encode putative polypeptides with nine transmembrane domains, indicating their possible functions are receptors or transporters (Chai, Locke et al. 2003). One study has shown that mutations of *NIPA1* gene in human cause autosomal dominant hereditary spastic paraplegia (Rainier, Chai et al. 2003). My study is mainly focused on the *Cyfip1* gene at the *l7Rl1* locus.

The genetic function of *Cyfip1*

Cyfip1, also called *Shyc* (selective hybridizing clone) in mouse and *SRA1* (specifically Rac1-associated protein) in human, belongs to a widely expressed and highly conserved gene family and its homologues have been identified in various organisms: *Arabidopsis*, *Dictyostelium*, *Caenorhabditis elegans*, *Drosophila melanogaster*, *Xenopus*, zebra fish, mouse and human (Basu, El-Assal Sel et al. 2004;

Figure 1.4. Schematic maps of human chromosome 15q11-q13 and the homologous mouse chromosome 7C region.

The black line represents the human chromosome 15q11-q13 or mouse chromosome 7C region. The direction of centromere and telomere is as indicated. BP1, BP2 and BP3 stand for the most three common chromosome break points in patients with PWS/AS. Genes in the homologous region or related to the study are showing as color dots on the chromosome. The color code is listed below the chromosome line.

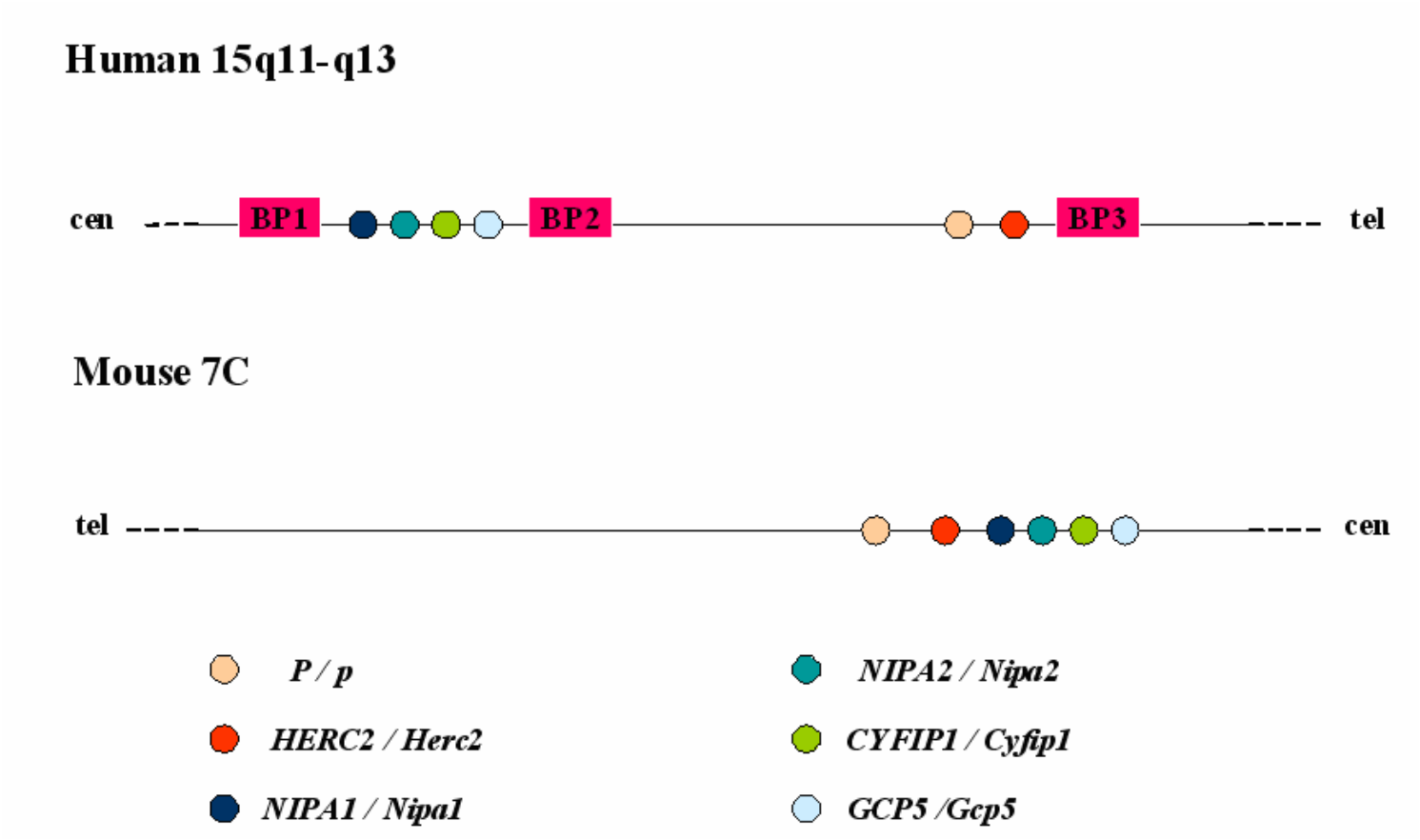
Human 15q11-q13
cen
BP1
BP2
BP3
tel
Mouse 7C
tel
cen
P / p
HERC2 / Herc2
NIPA1 / Nipa1
NIPA2 / Nipa2
CYFIP1 / Cyfip1
GCP5 /Gcp5

Soto, Qadota et al. 2002; Blagg, Stewart et al. 2003; Kobayashi, Kuroda et al. 1998; Koster, Schinke et al. 1998). *Cyfip1* was identified in mouse via screening an adult brain cDNA library for the neuronal differentiation process (Koster, Schinke et al. 1998). The *Cyfip1* gene has 31 exons, which encode a protein containing 1253 amino acid. Hydrophobicity analysis indicates that Cyfip1 is a hydrophilic 140 kDa protein localized at the cytoplasm. The function of Cyfip1 in the mammalian system is largely unknown, although the functions of its homologs have been studied in other organisms. Only one member of this gene exists in lower organisms, whereas two members of this gene family exist in mammals, *Cyfip1* and *Cyfip2* [also called P*IR121* (p53 inducible mRNA 121) in human]. Phylogenetic study of Cyfip1 protein reveals that the human CYFIP1 and CYFIP2 proteins share 98.7% and 99.9% of amino acid sequence identity to their corresponding mouse homologues, and 51% of amino acid sequence identity to fly and worm homologues, respectively (Figure 1.5). The genetic functions of Cyfip1 orthologs have been studied in different organisms. Although the function of CYFIP1 needs to be elucidated further in mammalian organisms, its function can be predicted from the role of its counterpart in other organisms.

In *Arabidopsis*, deletion of the Cyfip1 ortholog, *PIR* (*PIROGI)*, causes a disruption in remodeling of the actin cytoskeleton, malfunction of maintaining the polarized elongation of branched, hair-like cells, leading to epidermal cell-cell adhesion, and a phenotype of a well-stuffed pirogi and reduced fresh weight (Table 1.1). Although *PIR* shares less than 30% amino acid identity with human *CYFIP2*, interestingly, PIR is functional replaceable by human CYFIP2 in mutation rescue experiment. Furthermore,

Table 1.1 The gene function of CYFIP1 orthologs in different organisms

Organisms	Gene ortholog	Amino acid identity	Functions	Reference
Arabidopsis (Plant)	PIROG1	30%	Remodeling the actin cytoskeleton; maintaining the polarized elongation of branched, hair-like cells.	Basu et al., 2004
Dictyostelium (slime mold)	pirA	35%	Regulating actin dynamics in the formation of pseudopod;	Blagg et al., 2003
C. elegens (Worm)	GEX-2	51%	Tissue organization; Require for cells morphology and migration	Soto et al., 2002
Drosophila (Fly)	CYFIP/Sra-1	67%	Neuronal development. Require for axon growth, branching, and pathfinding, and maintain the structure in neuromuscular junction.	Schenck et al., 2003
Mouse	Cyfip1 /Shyc	-	Expressed in embryonic nervous system, and olfactory pathway in adult brain.	Koster et al., 1998
	Cyfip 2	88%	Function unknown.	Schenck et al., 2001
Human	Cyfip1/ Sra1	98.7%	Unknown	Schenck et al., 2001
	pir 121	99.9% to Cyfip2	Unknown	

Figure 1.5 Phylogenetic relationship of Cyfip1/2 from different organisms.

The numbers on the bottom indicate the percentage of nucleotide substitutions. The species and corresponding references are as follows: AAW51477 is human CYFIP1 protein; AF072697 is mouse Cyfip1 protein; AAH77907* is partial Cyfip protein in *Xenopus*; NP_99792 is the Cyfip protein in Zebra-fish; BC011762 is CYFIP2 protein in human; AF334144 is Cfyip2 protein in mouse; AAG61254 is dCYFIP protein in *Drosophila*; AB073209 is GEX-2 in *Caenorhabditis*; AAR89379 is pirA in *Dictyostelium*; and AAT71307 is PIROG1 in *Arabidopsis*.

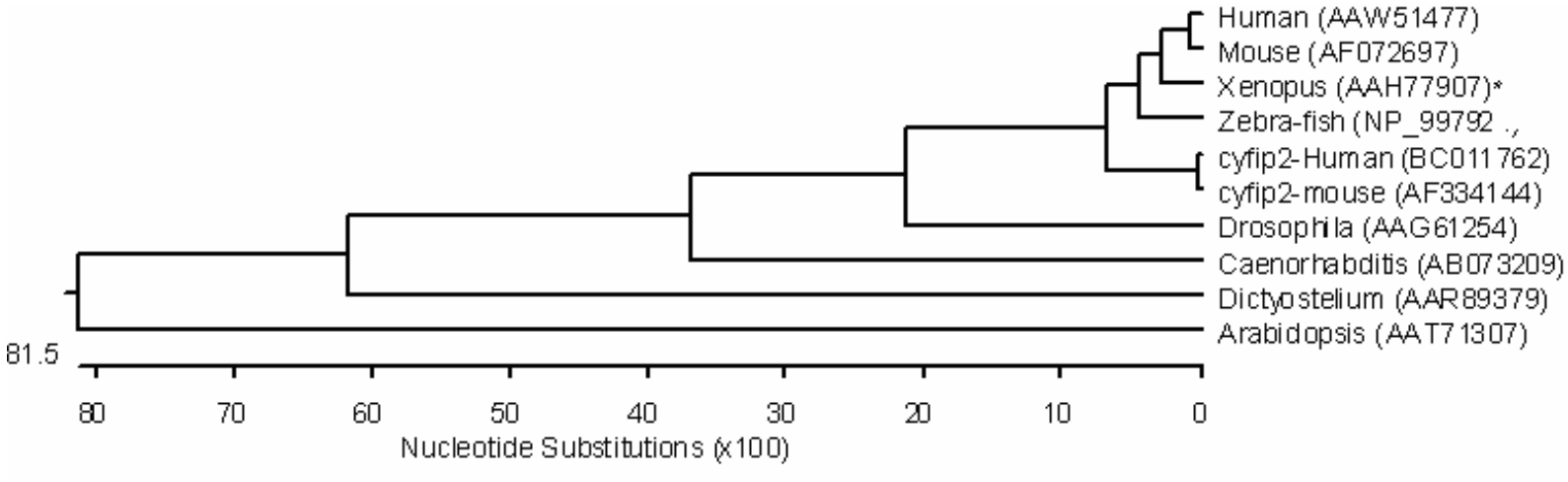
Human (AAW51477)
Mouse (AF072697)
Xenopus (AAH77907)*
Zebra-fish (NP_99792 .,
cyfip2-Human (BC011762)
cyfip2-mouse (AF334144)
Drosophila (AAG61254)
Caenorhabditis (AB073209)
Dictyostelium (AAR89379)
Arabidopsis (AAT71307)
81.5
80
70
60
50
40
30
20
10
0
Nucleotide Substitutions (x100)

similar to CYFIP1/SRA1, PIROGI encoded protein directly interacts with the RHO GTPases and SRA1 binding protein (Basu, El-Assal Sel et al. 2004).

In the slime mold *Dictyostelim*, *PirA* shares 35% amino acid identity to *Cyfip1*. *PirA* regulates the dynamics of actin polymerization process. Deletion of *PirA* results in accumulation of polymerized actin, resulting in an inability to form new pseudopods at new locations other than widening and splitting from existing pseudopods, which lead to defects in movement and chemotaxis (Blagg, Stewart et al. 2003)(Table 1.1).

In C. *elegans*, G*EX-2* (*gut on exterior protein 2*) shares 51% amino acid identity to C*yfip1*, and is involved in embryonic development and neuronal development. G*EX-2* is required for tissue morphogenesis and cell migration. In the absence of *GEX-2*, mutant embryos undergo gastrulation and cell differentiation. However, tissues fail to organize properly. For example, the formed intestinal cells fail to be organized in proper morphology, and are not able to migrate to their target locations in the initial steps of body morphogenesis (Soto, Qadota et al. 2002)(Table 1.1).

In *Drosophila*, dCYFIP shows 67% identity to mouse Cyfip1. It is highly expressed in neurons and involved in neuronal development. Mutations of dCYFIP are embryonic lethal, and lead to the central and peripheral nervous system abnormalities in axon growth, branching, and pathfinding. In particular, synapse terminals become shorter and neuronal morphogenesis such as axonal pathfinding (midline crossing), growth (motor axon stalling), branching (ectopic motor axon branching) are disrupted. In addition, the gene mutation also results in defects in the organization of neuromuscular junction structure (Schenck, Bardoni et al. 2003)(Table 1.1).

In mouse, *Cyfip1* is widely expressed during embryonic development. *In situ* hybridization experiments showed that the expression of *Cyfip1* can be detected in all three germ layers of developing mouse embryos at E7.5. Then, expression becomes stronger in the edges of the neural fold at E8.5. At E10.5, increased expression is seen in the mesoderm. The expression is reduced in the central nervous system and the transcripts are detected in the ganglia of the peripheral nervous system at E14.5. Also, strong expression signals are detected in the facial mesoderm, lung, gut, and the muscles, but not liver. At E16.5, major signals are detected in the peripheral nervous system and tooth anlage. In addition, transcripts are present in the central nervous system. In adult brain, expression is detected in the olfactory system, cerebral cortex, and Purkinje cells of the cerebellum (Koster, Schinke et al. 1998).

The wide expression of *Cyfip1* in the central nervous system of the early embryonic stage is conserved to the orthologs in *C. elegans* and *Drosophila*, which indicates the gene might plays an important role in mouse embryogenesis and the neuroectodermal differentiation process. Furthermore, the functional analysis of Cyfip1 ortholog suggests that Cyfip1 protein is likely involved in actin assembly, regulation of cellular morphology, and cell migration.

Protein-protein interaction of Cyfip1 with other proteins and signal transduction pathway

The regulation of cellular functions is carried out by signal transduction through protein-protein interaction. Cyfip1 function is reflected in the SCAR protein complex and in Cyfip1-FMRP interaction.

Actin polymerization process is essential for cellular morphology and mobility, and is of considerable important for cell survival and tissue organization. The generation of actin structure is through a protein complex pathway involving SCAR (suppressor of cAMP receptor), WAVE [WASP (Wiskott- Aldrich syndrome protein)-family verprolin homology protein], Arp2/3 (actin-related protein 2/3). The cycle of actin polymerization and depolymerization is regulated by the activated GTPase via promoting the activation of SCAR/WAVE protein complex. This is supported by the evidence that purified SCAR is constitutively active *in vitro* (Machesky, Mullins et al. 1999; Machesky and Insall 1998; Higgs and Pollard 1999), and inhibitory SCAR complex isolated from mammalian brain extracts responds to Rac signaling. In the inactive state, SCAR activity is restricted by the inhibitory SCAR complex, but the activation is dependent on the Rho-family GTPases, such as Rac GTPase. Upon addition of Rac-GTP, the inhibitory SCAR complex is dissociated in the actin polymerization process, which leads to free SCAR and another highly conserved actin regulator, HSPC300 (heat shock protein C300). SCAR and WAVE complex further activates a major nucleator of, actin polymerization, Arp2/3 complex, to form of new actin filaments (Machesky and Insall 1998; Higgs and Pollard 1999) SCAR coordinates actin reorganization by responding to Rac signal in the cell, but it does not directly bind to Rac GTPase (Pollard and Borisy 2003).

It is well established that GTP-loaded Rac1 (Regulating actin cytoskeleton protein 1) induces actin based plasma membrane projections such as lamellipodia and membrane ruffles by activating the Arp2/3 complex via SCAR protein (Miki, Suetsugu et al. 1998; Ridley 2001). Rac1 is a small GTPase belonging to a member of Rho subfamily. Rho-like GTPases, which function as molecular switches by cycling from an active GTP-bound

state to an inactive GDP-bound state. The function of this switch is to regulate the transmission of an extracellular signal to a downstream signaling pathway. This is achieved by the selective binding of the active GTPase to the downstream effector protein. In the cytosol of the resting cells, Rho-like GTPase, such as Rac1, is present in the GDP-bound form, stabilized by GDP dissociation inhibitor (GDI). When the cells are stimulated by certain upstream signal, the action of GDP/GTP exchange factor (GEF) results in the dissociation of GDI; then the GTP-bound form of Rho-like GTPase interacts with its specific downstream targets, thereby leading to the transmission of the signal. Rac1 has been found to regulate signal transduction pathways that mediate distinct cytoskeletal rearrangements required for cellular motility and cell migration (Figure 1.6) (Hall 1998).

Several lines of evidence suggest that Cyfip1 plays an important role in the SCAR-involved actin assembly process. First, a study of SCAR complex in its inactive state found that Cyfip1/Sra1/PIR121/CYFIP/GEX2 is a component of the complex (Eden, Rohatgi et al. 2002). In addition, using an affinity purification method, Cyfip1/Sra1 was identified from bovine brain cytosol as a downstream target of Rac1, for Cyfip1/Sra1 specifically interaction with the active form, but not with the inactive form of this small GTPase (Kobayashi, Kuroda et al. 1998). Thus, as an indispensable component of the SCAR complex, it is believed that Cyfip1 is responsible for SCAR complex activation in response to signaling molecules (Figure 1.6).

Cyfip1 function is also reflected in the Cyfip1-FMRP (fragile X mental retardation protein), protein interaction. Fragile X syndrome is an X-linked genetic disease. The disease is usually caused by the absence of the RNA binding FMRP, the

Figure 1. 6 Current understanding of Cyfip1/2 functions in the protein net-work (Modified from P. Billuart and J. Chelly)

In the SCAR - Arp2/3 complex pathway, CYFIP is an indispensable component of the inactive SCAR complex. During the presence of RAC-GTP, CYFIP interacts with RAC-GTP and release the active SCAR sub-complex. The SCAR then activates the Arp2/3 complex resulting in atcin nucleation. CYFIP might also act as a suppressor of FMRP by prevents its dimerization. RAC-GTP binds to CFYIP, free FMRP to form dimmer and exert its function as a negative translational regulator. Thus, CYFIP is likely to link RAC-dependent cytoskeleton remodeling and FMRP-dependent control of translation in a unique pathway.

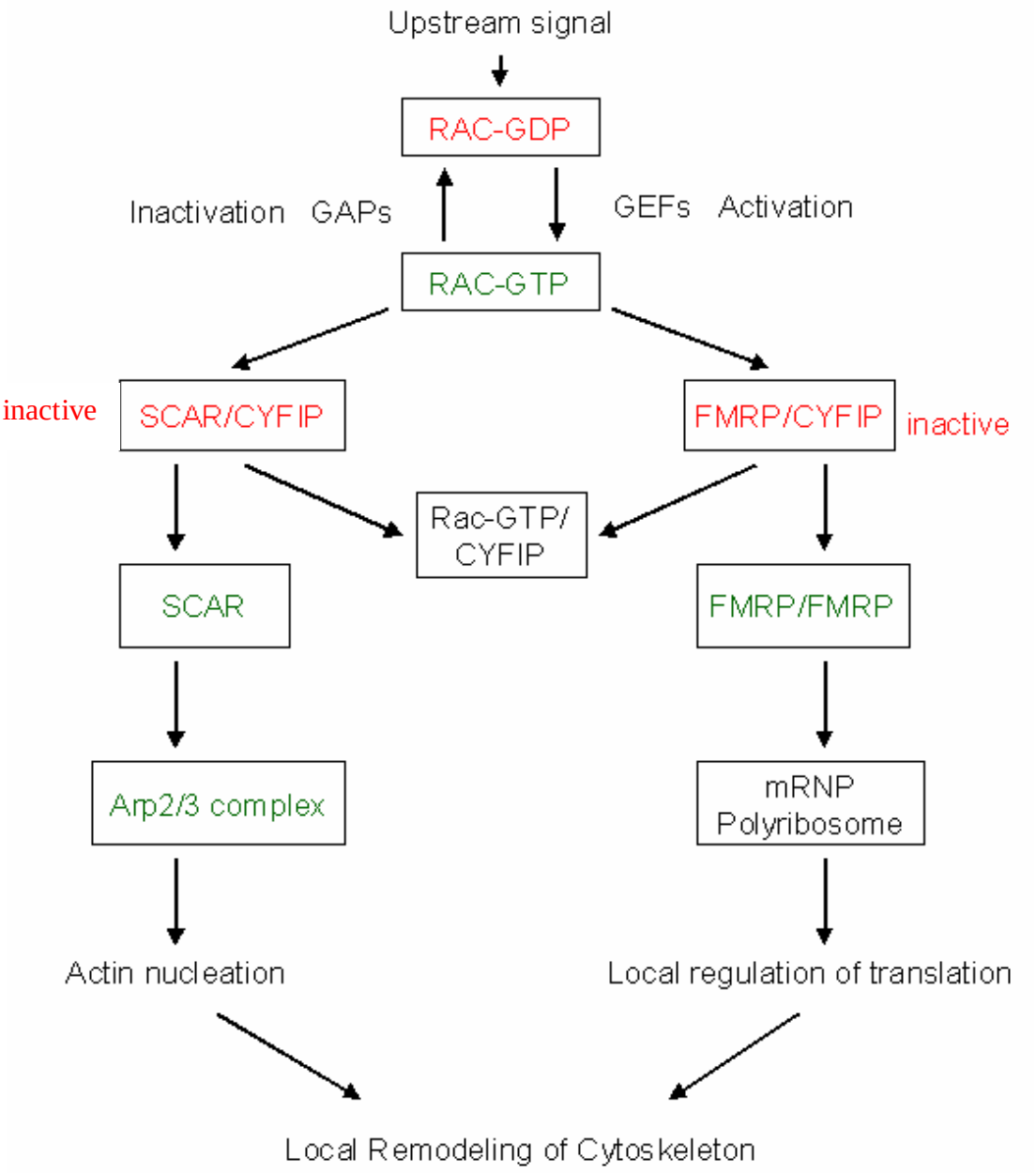
Upstream signal
RAC-GDP
Inactivation
GAPs
GEFs
Activation
RAC-GTP
inactive
SCAR/CYFIP
FMRP/CYFIP
inactive
Rac-GTP/
CYFIP
SCAR
FMRP/FMRP
Arp2/3 complex
mRNP
Polyribosome
Actin nucleation
Local regulation of translation
Local Remodeling of Cytoskeleton

protein product of *FMR1* gene (fragile X mental retardation 1), which leads to the presence of a cytogenetically visible fragile site on chromosome X (For review see (Bardoni, Schenck et al. 2001). The FMRP protein is highly conserved in vertebrates and belongs to a family that contains two other proteins: FXR1 and FXR2 (fragile X related protein 1 and 2). Studies have shown that FMRP functions as a negative translational regulator, and the dimerization of FMRP is essential for its function (Laggerbauer, Ostareck et al. 2001; Li, Zhang et al. 2001; Schaeffer, Bardoni et al. 2001). FMRP dimerization occurs in the cytoplasm, and can be a homorization of FMRP-FMRP or heteromerization of FMRP-FXR (Siomi, Siomi et al. 1995)

Cyfip1/Sra1 is found to interact with FMRP in a yeast two hybrid screening, in which a mouse embryonic cDNA library was screened with the highly conserved N terminus of FMRP as bait (Schenck, Bardoni et al. 2001). The region of FMRP important for its dimerization is also responsible for its interaction with Cyfip1. In another words, the interaction region of Cyfip1 and FMRP overlaps with the homo/heteromerization domain of FMRP (Schenck, Bardoni et al. 2001; Siomi, Zhang et al. 1996). Since dimerization is an important step for FMRP to exert its function, it is suggested that Cyfip1 act as a suppressor of FMRP by binding to FMRP to prevent its dimerization (Billuart and Chelly 2003). Cyfip1 does not interact with FMRP-related proteins FXR1/FXR2, despite their high sequence similarity with FMRP. Cyfip2, the cyfip1 homolog in mammal, is also capable of interacting with FMRP. But unlike the exclusive interaction between Cyfip1 and FMRP, Cyfip2 interacts with FXR1 and FXR2 as well (Schenck, Bardoni et al. 2001).

A study in *Drosophila* provides evidence that CYFIP links Rac-dependent cytoskeleton remodeling and FMRP-dependent control of translation in a common pathway (Schenck, Bardoni et al. 2003). The *Drosophila* genome contains a single ortholog of the human *FXR* gene family (*dFMR1*) and its biochemical properties and role is conserved in the fly nervous system (Wan, Dockendorff et al. 2000; Zhang, Bailey et al. 2001; Dockendorff, Su et al. 2002; Morales, Hiesinger et al. 2002; Schenck, Van de Bor et al. 2002). A single fly *CYFIP* gene, *dCYFIP*, has been identified as the fly ortholog of human CYFIP1 and CYFIP2 (Schenck, Bardoni et al. 2001). The biochemical interactions between dCYFIP and dFMR1 or dRac1 are conserved in fly and these interactions are exclusive to each other. The study suggests dCYFIP might present in two alternative complexes, associated with either dFMR1 or with dRac1. Genetic interaction experiments in eye and nervous system show that dCYFIP antagonizes dRac1 and dFMR1. These data, together with the fact that dCYFIP, dRac1 and dFMR1 mutants share lots of similiar defects (Dockendorff, Su et al. 2002; Morales, Hiesinger et al. 2002; Hakeda-Suzuki, Ng et al. 2002; Kaufmann, Wills et al. 1998; Ng, Nardine et al. 2002) suggest a model in which CYFIP proteins and Rac1 might be part of a pathway regulating both cytoskeleton remodeling and FMRP-dependent control of translation (Figure 1.6).

Rationale for this study

This study was undertaken to identify possible gene resulting in the peri-implantation lethality in *l7Rl1* locus. Among the four genes mapped to *l7Rl1*, *Cyfip1* is expressed at all three germ layers in the early mouse embryo development, and null

mutations of the gene in worm and fly result in early embryonic lethality. Therefore, we hypothesize that *Cyfip1* is the gene responsible for the l7Rl1 null phenotype. We focus on characterization of the phenotype of the homozygous *Cyfip1* gene-trapped embryos; analysis of two pre-mapped ENU-induced mutations; and identification of genetic alteration of the two mutations and the corresponded genetic mechanisms.

CHAPTER II

GENERATION AND CHARACTERIZATION OF A *Cyfip1* GENE-TRAP MUTATION

INTRODUCTION

Early miscarriage is the spontaneous loss of pregnancy during the first 20 weeks of gestation in human. It occurs in 15-20% of all conceptions, and as many as 30% of women will experience one, usually before they even miss a period, or realize they are pregnant. Some women even suffer from Recurrent Miscarriage (RM), defined as three or more miscarriage during the first trimester. Most early miscarriages remain unexplained. In mammals, embryonic development is a complex process involving cell proliferation, cell differentiation, organogenesis and tissue differentiation, as well as morphological changes (Rugh 1994 and Hogan, 1994). Disturbance in any of these processes results in either embryonic lethality or malformation of the fetus. Other than the mother's physical condition, it is usually assumed these losses are results of genetic defects. Studying the deficiency of embryonic development using mouse mutants and exploring the genetic mechanisms will promote our understanding on the early embryonic development.

As described in the previous section, *l7Rl1* is a locus mapped as a functional unit related to an early post-implantation lethal. Homozygous deletion mutation of the locus leads to embryonic lethality at the time of implantation; therefore, this genetic region is required for peri-implantation survival in the mouse (Russell, Montgomery et al. 1995; Wu, Rinchik et al. 2000). The minimum critical region of *l7Rl1* is narrowed down into

~300kb (Wu, Rinchik et al. 2000) and contains genes(from centromere to telomere): *Tubgcp5*, *Cyfip1*, *Nipa2*, and *Nipa1*(Chai, Locke et al. 2003). Since the locus contains more than one gene, it remains to be solved which gene(s) and how the gene(s) contributes to the implantation failure.

Among the four genes mapped in the *l7Rl1* locus, *Cyfip1* shows close relation to the embryonic development (Koster, Schinke et al. 1998; Soto, Qadota et al. 2002; Schenck, Bardoni et al. 2003). *Cyfip1* belongs to a highly conserved gene family, and its orthologs have been identified in various organisms (Soto, Qadota et al. 2002; Basu, El-Assal Sel et al. 2004; Koster, Schinke et al. 1998; Blagg, Stewart et al. 2003; Schenck, Bardoni et al. 2003; Kobayashi, Kuroda et al. 1998). Functional studies of *Cyfip1* orthologs show that null mutation of this gene in worm and fly results in early embryonic lethality (Soto, Qadota et al. 2002; Schenck, Bardoni et al. 2003).. In mouse, *Cyfip1* is widely expressed during the mouse embryonic development (Koster, Schinke et al. 1998). We hypothesize that *Cyfip1* is a candidate gene among the four causing the peri-implantation lethal phenotype.

To study the function of *Cyfip1*, a *Cyfip1* gene-trap ES cell line carried by the BayGenomics gene-trap facility (http://baygenomics.ucsf.edu) was used to generate homozygous *Cyfip1* gene-trap mice. In the study, $Cyfip1^{Gt/+}$ chimeric mice were first derived from the gene-trap ES cell clone and heterozygous gene-trap offspring were generated. From crossing of $Cyfip1^{Gt/+}$ heterozygotes, the homozygous $Cyfip1^{Gt/Gt}$ embryos were obtained and characterized. We compared the mouse embryonic development of $Cyfip1^{Gt/Gt}$ with that of homozygous deletion of *l7Rl1* locus, particularly

in the early stage of mouse embryonic development, and answer whether the disruption of *Cyfip1* is sufficient to cause peri-implantation failure.

Embryo development of the Mouse

As a model organism, mouse embryo development has been well studied and understood. The mouse gestation period is usually 19 days, with the range from 18 to 21 in different strains. Same as other vertebrates, the intrauterine development falls into three consecutive phases: (1) primary development from fertilization through germ layer derivation, (2) basic organogenesis, and (3) tissue differentiation with functional maturity and organismic integration. The first period lasts about 6 days. By the end of 6dpc, the implantation of embryo is completed. The second stage takes about 6 days as well, although some organ systems are not fully differentiated until after birth (e.g., cerebellum, gonads); all major organ systems have been developed after this stage. In the third stage, the embryo further developed into fetus and is capable of independent life. The introduction here is focused on the development from 8dpc to 9.5dpc, for detailed reviews on mouse embryo development, see Rugh (1994) and Hogan et al. (1994) (Rugh 1994) (Hogan 1994).

The development of mouse embryo can be divided into 28 stages ((Kaufman 1989). Although embryos of the same gestation age may differ in their stage of development, gestational age 8, 8.5, 9 and 9.5 are generally consider as stage 12, 13, 14 and 15, respectively (Table 2. 1) (Bard 1998).

At stage 12, somites pairs first appear in the embryo. A somite is a block of dorsal mesodermal cells adjacent to the notochord during vertebrate organogenesis. As transient

Table 2.1 Important events occurring during mouse embryo development: stage 12- 15 (Kaufman 1989; Bard 1998)

Theiler Stage	dpc	Somite No.	Major events
12	8	1-7	1st somite appears; alloantois extends and contacts chorion at the end of the stage; 1st branchial arch become prominent; the heart starts to form; the headfords are prominent; neural closure occurs in the region of the 4th and 5th somites
13	8.5	8-12	Turning of the embryo; 2nd branchial arch presnet; regionalization of the heart ; the neural tube is closed from a point opposite the outflow tract to the proximal part of the tail
14	9	13-20	Formation & closure of anterior neuropore; the neural tube is closed except for the posterior neuropore; the otic pit indented but not closed; the 3rd branchial arch becomes visible late in the stage
15	9.5	21-29	Formation of the posterior neuropore; forebrain vesicle subdivides; the primitive streak has disappeared; the forelimb bud becomes apparent near the 8th to 12th somites pairs

structures, somites define the segmental pattern of the embryo, and subsequently give rise to vertebrae and ribs, dermis of the back, and the skeletal muscles of the back, body wall and limbs. The 8 day embryo can be identified by its 4 pairs of somites, but the number can range from 1 to 7 pairs. The maxiliary components fo the 1st branchial arch become prominent. The cardiogenic plate begins to form and develops rapidly. The headfolds are particularly prominent and neural closure occurs in the region of the 4th and 5th somites, extending in both directions from this site. The allantois extends further into the exocoelom and contacts the chorion at the end of this stage (Downes 1993).

At 8.5 gestation, a major activity undergoing is the initiation of the turning process in the embryo. Growth of the foregut and hindgut initiates the reversal of the anterior-posterior relationships. The head end is turning clockwise while posterior regions are turning counterclockwise. The midgut remains connected with the yolk cavity but also rotates rapidly. The embryo eventually acquires the C shape characteristic of most vertebrate embryos, with the open part of the C ventrally directed (Rugh 1994). Stage 13 usually starts with 6 to 8 pairs of somites and completes in embryos with 14 to16 pairs of somites. A second branchial arch is now evident. There is evidence of regionalization of the heart and the neural tube is closed from a point opposite the outflow tract to the proximal part of the tail.

Between 8.5 to 9 days, the most significant and involved changes occur in the embryo, when the organogenesis is greatly accelerated and the contour of the embryos is being altered simultaneously. The stage 14 embryo has 13 to 20 somites. The neural tube is closed except for the posterior neuropore and the roof of the myelencephalon, and the entire nervous system is undergoing cellular differentiation. The otic pit becomes

progressively more indented but not closed, and the mandibular process of the 1st branchial arch is clearly visible. The 3rd branchial arch becomes visible late in the stage (Rugh 1994).

The stage 15 embryo has 21 to 29 somites. The reversal of the original lordosis of the back now brings the telencephalon and tail into close approximation. The head is far in advance of the rest of the body in development. The four major divisions of the brain are apparent from the surface. The primitive streak has disappeared by incorporated into the embryo. The posterior neuropore forms. The condensation of the forelimb bud becomes apparent near the 8th to 12th somites pairs. A distinct condensation of the hind limb bud appears just at the end of the stage.

MATERIALS AND METHODS

Cyfip1 gene-trap ES cell line

The *Cyfip1* gene-trap ES cell line (XG769) was purchased from the BayGenomics Date Base (http://baygenomics.ucsf.edu). The gene-trap vector inserted is pGT1Lxf, which contains a ß-geo cassette. The trace data from this clone aligns to exon 12 of *Cyfip1*, indicating that the gene-trap vector should be inserted between exon 12 and exon 13.

Generation of *Cyfip1* gene-trap transgenic mouse

All animals used in this study were bred at the mouse facility at Oak Ridge National Laboratory. XG769 ES cells were cultured by an established protocol without

feeders (Ramirez-Solis, 1993). To harvest blastocysts, C57BL/6 female mice were naturally mated and sacrificed at 3.5dpc. Isolated uteri were flushed with ES cell media. The cultured ES cells were injected into the inner cell mass of the blastocysts, and then the blastocysts carrying ES cells were transferred to the uterine horn of 2.5 dpc pseudopregnant B6 females to generate chimeras. This work was performed by Sarah Mentzer.

Identification of mice carrying the gene-trap allele

Chimeric males were crossed to C57BL/6, and pups carrying the gene-trap allele were identified by PCR of *neo* gene sequences using genomic DNA from ear clips as template. The resulting *Cyfip1*$^{Gt(pGT1Lxf)1You/+}$ heterozygotes (abbreviated to *Cyfip1*$^{Gt/+}$) were crossed to B6 for one to three generations before heterozygotes were intercrossed. Primers used for genotyping were Neo3F: 5'-AGGATCTCCTGTCATCTCACCTT-3'; Neo3R: 5'-CACAGTCGATGAATCCAGAAAAG-3'. PCR parameters were: 94°C 4 min; 39 cycle of 94°C 30 sec, 60°C 30 sec, 72°C 45 sec; 7 2°C 10 min; and 4°C hold.

Total RNA isolation and Northern Blot hybridization

XG769 and Dnm2 (a *Cyfip1*$^{+/+}$ gene-trap ES cell line used as control) ES cell were grown to confluence in 25mm flask and total RNA was isolated from the cells using the standard Trizol method. Total RNA of *Cyfip1*$^{Gt/+}$ or wild-type mouse was isolated from mouse spleen,which was snap-frozen in liquid N_2, by the Trizol method (Eppendorf-5 prime, Inc. Boulder, CO).

For Northern blot analysis, 20µg of total RNA of wild type or Cyfip1$^{Gt/+}$ was loaded per lane into a formaldehyde-reducing gel. Gels were run in buffer containing MOPS (pH 7.0) for 5 hours at 75V and then transferred by capillary action onto a nylon hybridization membrane in 10x SSC. Total RNA was UV cross-linked to the membrane with a Stratalinker UV source. The blot was prehybridized at 65°C in a buffer (7% SDS, 1% BSA, 1mM EDTA, and 250 mM Na_2HPO4, pH 7.2) for 2 hours and hybridized overnight in the same buffer containing radioactive probes at 65°C. Radioactive probes were prepared as follows. A 1 kb fragment was obtained by PCR amplification using the primers: Shyc3-1F (5'-AGATACATCGAACAAGCAACTGTC-3') and Shyc11/12-1R (5'-TACAGCAATAGCGAGGTAGTCACA-3'). DNA fragments were labeled with (α-^{32}P)-dATP by random-primed probe synthesis. Blots were rinsed with post-hybridization buffer (0.1X SSC, 0.1% SDS) at 65°C, and the RNA images were developed with a Storm 840 phosphoimager (Molecular Dynamics, Sunnyvale, CA).

Reverse transcript and PCR analysis of the gene-trap transcript

Total RNA was extracted as described above. cDNA was synthesized by using Superscript III reverse transcriptase (Invitrogen's SuperScript® First-Strand Synthesis System). The synthesized cDNA was purified using QIAGEN quick PCR purification kit following the manufacturer's instructions and stored at -20°C until required. First strand cDNA from the XG769 and Dnm2 ES cells was used directly for PCR analysis. Primers: Shyc12-1F (5'-AGCCCAGAAGACAGATGCTGAGTA-3'), Shyc18-1R (5'-ATGGAGTACGTCCTCTACTCCTTG-3'), and GT-β-reverse (5'-CGATCTTCCTGAGGCCGATACTGTC-3') were chosen for the PCR to detect the

hypothetic insertion of gene trap. PCR parameters were: 96°C 5 min; 39 cycles of 96°C 30 sec, 55°C 30 sec, 72°C 30 sec; 72°C 10min; 4°C hold.

Embryo observation and histology

Cyfip1$^{Gt/+}$ mice were intercrossed to obtain homozygous gene-trap mutant embryos (*Cyfip1*$^{Gt/Gt}$). Mice were naturally mated, and the day of the vaginal plug found was considered to be 0.5dpc. Uteri of pregnant females were dissected in 1 x PBS at embryonic days 8.5, 9.5, 10.5 and 11.5. Embryo dissection followed the protocol described in Nagy *et al*., 2003 (Manipulating the Mouse Embryo).

For histological sections, dissected embryos were fixed overnight in ice-cold 4% paraformaldehyde (EMS) in PBS, then were dehydrated through a graded ethanol series and embedded in paraffin. The embedded embryos were sectioned and generated 5-7μm thick cross-section and stained with haematoxylin/eosin.

The whole embryos and their cross-sections were photographed using a Zeiss SV11 dissection microscope and Spot 100 digital camera connected to a Macintosh computer.

Whole mount *in situ* hybridization

Embryos were dissected in PBS and fixed in ice-cold 4% paraformaldehyde overnight. Fixed embryos were then dehydrated through a graded series of methanol and stored in 100% methanol at -20°C before *in situ* hybridization. Probes of the brachyury (*T*) and fibroblast growth factor 8 (*Fgf8*) used in the whole mount *in situ* hybridization were obtained from Dr. H. Chao. Preparation of digoxigenin labeled RNA probe and whole

mount *in situ* hybridization was performed as described previously (Chao, Mentzer et al. 2003). After hybridization procedures, embryos were re-fixed in 0.1% glutaraldehyde solution at 4°C overnight and cleared first in 50% glycerol/PBS/0.01% sodium azide, then in 80% glycerol/PBS/0.01% sodium azide overnight. The embryos were photographed using a Zeiss SV11 dissection microscope and Spot 100 digital camera connected to a Macintosh computer.

RESULTS

Generation of *Cyfip1* gene-trap transgenic mouse

Gene-trap creates random insertion mutations in the genome, which are immediately accessible for molecular characterization. When carried out in ES cells, the gene-trap insertions transmit into the germ line of mice for analysis of the function of the trapped gene in *vivo*. To gain further understanding the function of *Cyfip1* in the *l7Rl1* locus, *Cyfip1* gene-trap transgenic mouse was generated. Gene-trap ES cells derived from 129 strain (agouti) were injected into C57Bl/6 blastocyst (black). For a particular mouse developed from the blastocyst carrying the gene-trap, the more of ES cells contribute to the genome, the greater of the amount of agouti is shown in the coat. The generated chimera mouse is usually “tiger” striped. Males carrying 40% to 100% of agouti coat color were mated with B6 (Figure 2.1), and their offspring were screened by PCR of *neo* gene sequences. Chimeric males which produced more than 6 litters without carrying of the transgene were not likely that the gene-trap goes to the germ line and were sacrificed.

Figure 2.1 Generation of *Cyfip1* transgenic mouse.

Cultured *Cyfip1*$^{Gt/+}$ ES cells from 129 strain (agouti) were injected into inner cell mass of harvested C57B1/6 (mice are black color) blastocysts, then the injected blastocysts were transferred to the uterine of the B6 foster mother. The more of the ES cells contribute to the genome, the more of the coat color is shown as agouti. The left panel is littermates from the foster mother. Mouse on the top: black mouse indicates no apparent ES cell contribution. Mouse in the middle: chimeric founder has high ES cell contribution. Mouse on the bottom: chimeric founder – weaker ES cell contribution. The right panel is a Cyfip1$^{Gt/+}$ male chimera with high ES cell contribution and the offspring. Offspring are further screened for transgene carriage.

Confirmation of the gene-trap effect

For the XG769 gene-trap ES cell line, the gene-trap vector was inserted into intron 12 of *Cyfip1* gene. The predicted transcript resulting from the insertion would be the first 12 exons of *Cyfip1* fused with the report gene ß-geo. All exons at the downstream of the insertion site were expected to be lost. Several approaches have been applied to confirm the gene-trap effect in XG769 gene-trap line. First, the cDNA synthesized from total RNA extraction of XG769 and Dnm2 ES cell lines was used for PCR analysis to confirm the existence of fusion gene-trap transcript. Three primers, a forward primer Shyc12-1F located in exon 12, a reverse primer Shyc18-1R located in exon 18, downstream of the gene-trap insertion, and the second reverse primer GT-β-reverse located in gene-trap vector pGT1Lxf, were mixed together in the same PCR reaction for the analysis. In Dnm2 ES cDNA template (wild type transcript), the primer pair Shcy12-1F and Shyc18-1R is expected to amplify 1Kb product only. In contrast, in XG769 cDNA template (heterozygous transcript), the three primers Shcy12-1F, Shyc18-1R and GT-β-reverse are expected to amplify one about 1Kb PCR product from the wild type transcript and one about 450bp PCR product from the gene-trap transcript. Gel electrophoresis of the PCR products confirmed the above hypothetic analysis (Figure 2.2).

Northern Blot analysis has also been applied to confirm the existence of gene-trap version of the transcript. Total RNA of *Cyfip1*$^{Gt/+}$ or wild type isolated from mouse spleen was used for this purpose. The probe used for the Northern Blot is a 1kb fragment located upstream of the gene-trap insertion. For the wild type RNA, the probe detected a single band at ~4kb, which should be the wild type *Cyfip1* transcript, while the same probe detected two bands from the *Cyfip1*$^{Gt/+}$ RNA. In addition to the wild type transcript, a

Figure 2.2 PCR analysis of the *Cyfip1*$^{Gt/+}$ cDNA.

cDNA was prepared from total RNA from XG769 and Dnm2 ES cells and amplified by PCR with specific primer pairs. A: Primers used for the PCR analysis. Primer pair Shyc12-1F and Shyc18-1R is designed for the wild-type transcript and primer pair Shyc12-1F and GT-β-reverse is designed for the gene-trap transcript. B: The PCR products were run in 0.8% agarose gel along with NEB 1Kb marker. The 1Kb marker was run on the most left lane of the gel; the middle lane was the PCR products by using Dnm2 cDNA as the template; the most right lane was the PCR products by using cDNA from XG769 ES cells as the template; the expected amplification products of the wild-type transcript (about 1Kb) and the gene-trap transcript (about 450bp) were shown.

A:

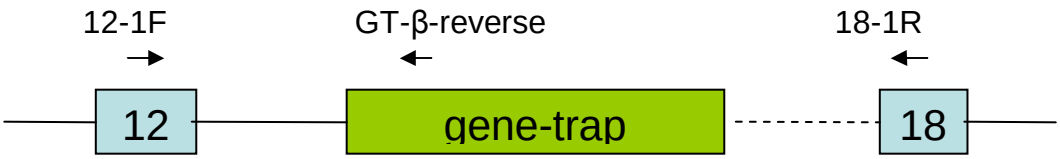
12-1F
GT-β-reverse
18-1R
12
gene-trap
18

B:

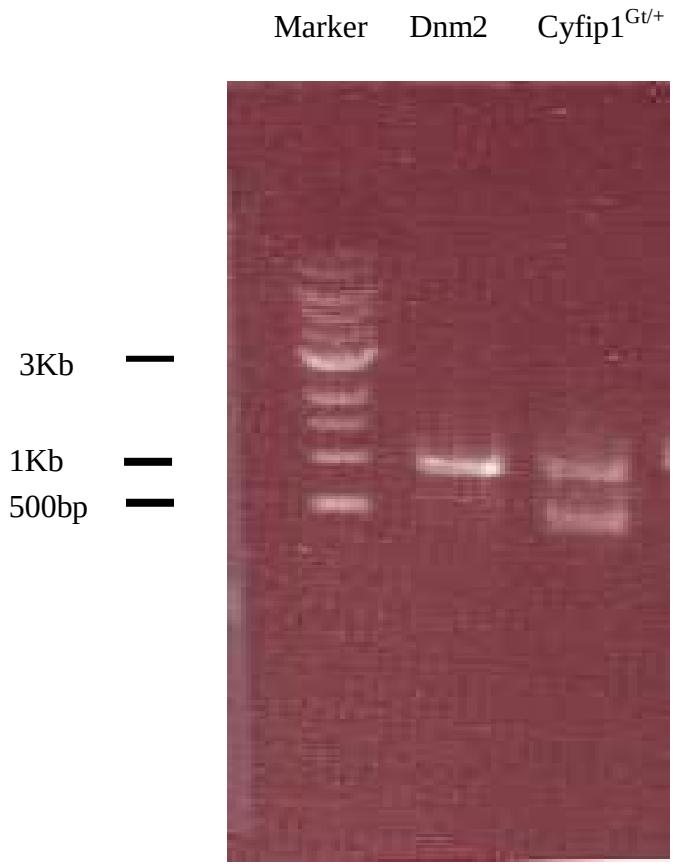
Marker
Dnm2
Cyfip1Gt/+
3Kb
1Kb
500bp

larger *Cyfip1* transcript has also been detected, which provided us direct evidence of the gene-trap effect (Figure 2.3).

Characterization of the phenotype of *Cyfip1*$^{Gt/Gt}$ mutant embryos

Heterozygous *Cyfip1*$^{Gt/+}$ mice generated from the gene-trap chimeric males were outwardly normal and fertile. Homologous gene-trap embryos were obtained by intercrossing *Cyfip1*$^{Gt/+}$ heterozygotes. Embryos were dissected at 8.5dpc, 9.5dpc and 11.5dpc, and examined. Furthermore, histological sections of 9.5dpc embryos from the intercrosses were studied. No resorbing moles in the conceptuses were observed at 8.5dpc, implying that homozygous *Cyfip1*$^{Gt/Gt}$ embryos were able to survive through the peri-implantation stage (4.5dpc-6.5dpc). In contrast, a total of 139 deciduas from the experimental mating were examined at 9.5dpc; 32 embryos showed significant developmental abnormality (23%), which agree with the Mendel's law that 25% abnormal embryos should be observed as the homozygous *Cyfip1*$^{Gt/Gt}$ mutant**.** At 11.5dpc, about 7 out of 26 (26.9%) deciduas showed no morphological evidence of embryonic development, indicating the mutant embryos had been disintegrated (Table 2.2).

During mouse embryo development, normal embryos start the embryonic turning at 8.5dpc. By 9.5dpc, the turning process is completely finished; approximately 23 pairs of somites should be presented and the neural tube should be closed (Rugh 1994; Downes 1993). In contrast to normal embryo development, *Cyfip1*$^{Gt/Gt}$ mutant embryos had only 6-12 somties at 9.5dpc, which is the somite number for the normal embryos at 8.5dpc, suggesting embryonic development arrest at around 8.5dpc. In addition, although the somite structures were visible, they appeared disorganized. Furthermore, the anterior-

Figure 2.3. Northern blot analysis of *Cyfip1*$^{Gt/+}$

Total RNA was prepared from wild type and *Cyfip1*$^{GT/+}$ mouse spleen and blot onto a nylon membrane. A ~1kb DNA fragment span exon 3 to exon 11 was used as the probe.

A: wild type and gene-trapped *Cyfip1* transcripts. The dark line above each transcript represents the probe used in the Northern Blot hybridization. B: Northern Blot analysis. The about 4kb *Cyfip1* transcript was detected from total RNA of the wild type, whereas two bands as we expected, one in about 4kb representing wild type *Cyfip1* transcript and one in about 8kb representing *Cyfip1*-gene-trap fusion transcript, were detected from the total RNA of *Cyfip1*$^{GT/+}$.

A:

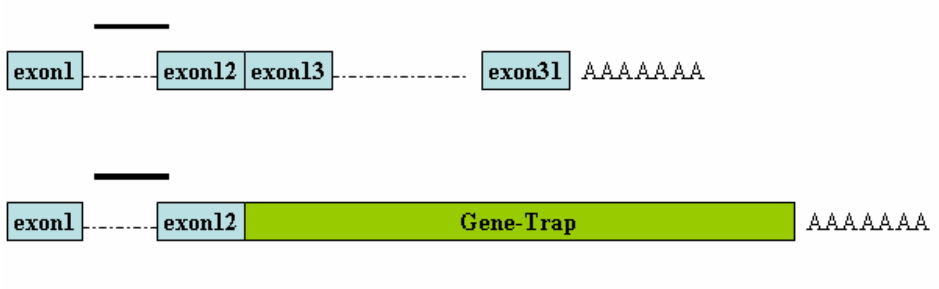
exon1
exon12
exon13
exon31
AAAAAAA
exon1
exon12
Gene-Trap
AAAAAAA

B:

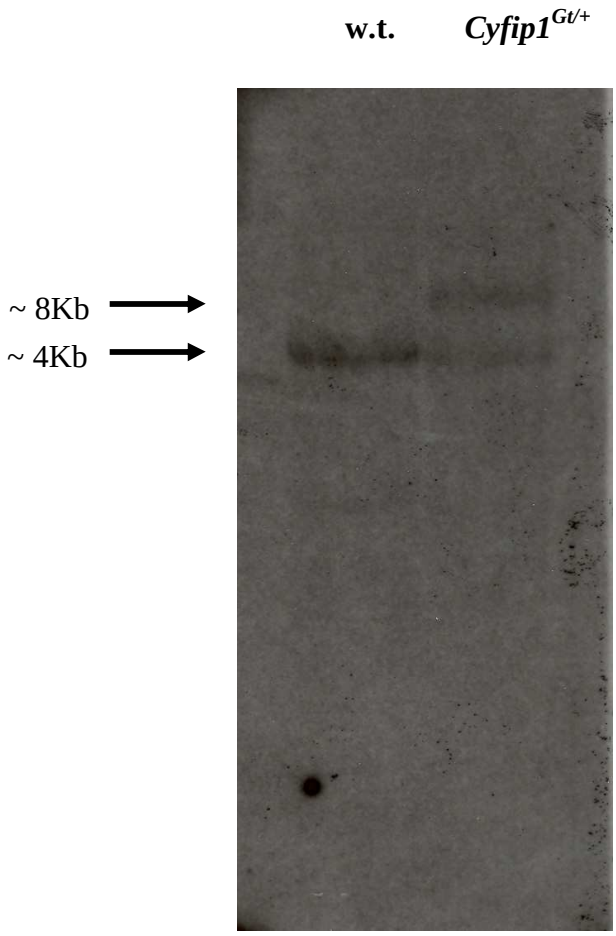
w.t.
Cyfip1Gt/+
~ 8Kb
~ 4Kb

Table 2.2 Results of uterine dissection from Cyfip1$^{Gt/+}$ x Cyfip1$^{Gt/+}$ mating

Age	Observed decidua	Number of empty decidua or abnormal embryos	% of empty or abnormal embryos
E8.5	43	0*	0% empty decidua
E9.5	139	32**	23%
E11.5	26	7*	26.9%

***number of empty deciduas**

****number of abnormal embryos**

posterior axis of the mutant embryos was not able to further elongate. The mutant embryos remained in lordotic position and displayed kinky neural tube and wavy developing brains. Finally, neural tube closure was not observed in mutant embryos by 9.5dpc (Figure 2.4 and Figure 2.5).

The site of primitive-streak formation during gastrulation marks the future posterior side of the embryo and thus defines the anterior-posterior axis. The anterior-posterior axis is positioned by coordinated cell movements and rotation from the pre-existing proximal-distal axis (Thomas and Beddington 1996; Ding, Yang et al. 1998; Rhinn, Dierich et al. 1998; Kimura, Yoshinaga et al. 2000). Since the mutant embryos displayed abnormalities in anterior-posterior axis elongation and embryonic turning, we performed mRNA whole mount *in situ* hybridization using probes of two different posterior markers, the *T* gene and *Fgf8* gene (Figure 2.6). The whole mount *in situ* hybridization results indicated that *T* gene expression pattern in 8.5dpc mutant embryo was similar to that in the wild-type littermates, but the expression of *Fgf8* was very low, if any, compared to its wild-type littermate at 9.5dpc. The *T* gene is known to play a direct role in mesoderm formation and in the morphogenesis of the notochord and *Fgf8* is essential in morphogenesis of the central nervous system during mouse embryo development (Inatani, Irie et al. 2003). The data suggested that the development and morphogenesis of the notochord in *Cyfip1*$^{Gt/Gt}$ mutant embryos has not been disrupted, whereas the defect of the central nervous system development is severe.

Figure 2.4 Morphology of wild-type and *Cyfip1*$^{Gt/Gt}$ mutant embryos.

Upper left panel: a presumably 9.5dpc *l7Rl1*$^{Gt/Gt}$ mutant embryo with its wild-type littermates. Mutant embryo is much smaller and under developed as comparing to the wild-type. Upper right panel: The enlarged dorsal view of the same mutant embryo. Lower left panel A: ventral view of a wild-type embryo at ~8.0dpc. The embryo has 8 pair of somites. The developing neural tube runs linearly up the midline of the embryo with somite pairs on either side. B: lateral view of littermates (9.5dpc, w.t. on the left, and mutant on the right) from the cross of Cyfip1$^{Gt/+}$ x Cyfip1$^{Gt/+}$ heterozygotes. The mutant embryo did develop somites (not clear in this image), but displayed a kinky neural tube and wavy developing brain. Arrows: neural tube. Arrowheads: somites. Scale bars: 0.5mm.

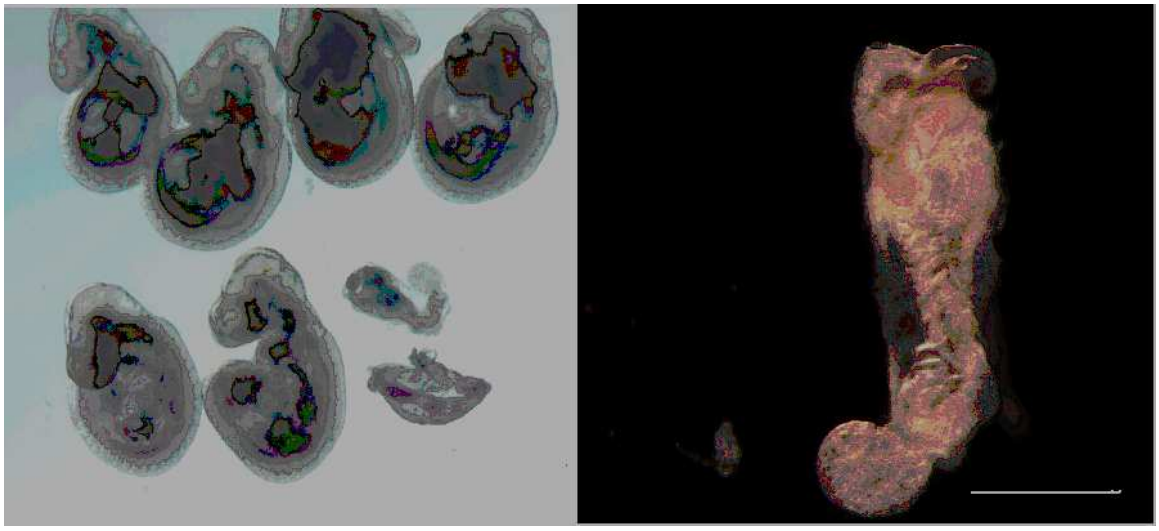

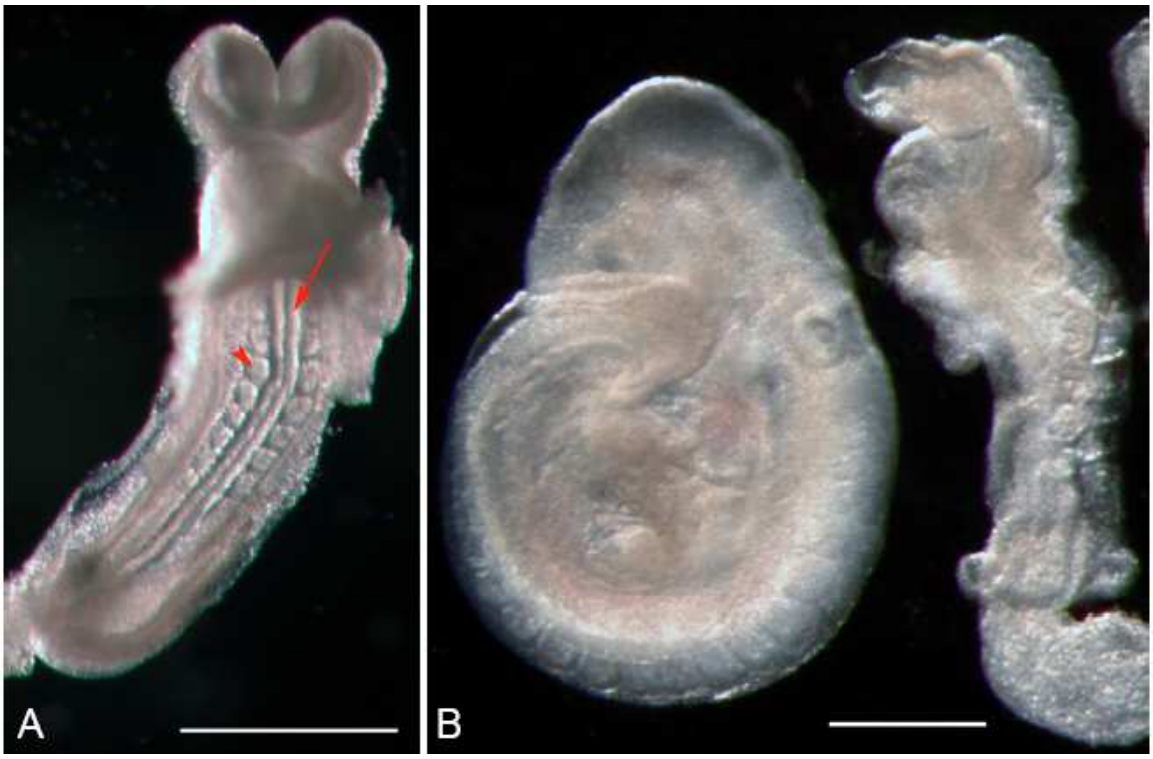
A
B

Figure 2.5 Histological section of wild-type and *Cyfip1*$^{Gt/Gt}$ mutant embryos

E: wild-type (left) and mutant (right) 9.0dpc embryos from a cross of *Cyfip1*$^{Gt/+}$ x *Cyfip1*$^{Gt/+}$ heterozygotes. Arrows and letters F, G, H indicate the section planes for the panels F-H. F: transverse section of the mutant embryo near the trunk region. The kinky neural tube (nt) and the disorganized somites (so) were clearly visible. G: Section near the foregut pocket showed kinky forebrain (fb). No neural tube closure was observed and the embryo was in lordotic position without embryonic turning. H: Section went through the developing heart (ht) showing it was at around 8.5dpc stage. Scale bars: 0.5mm.

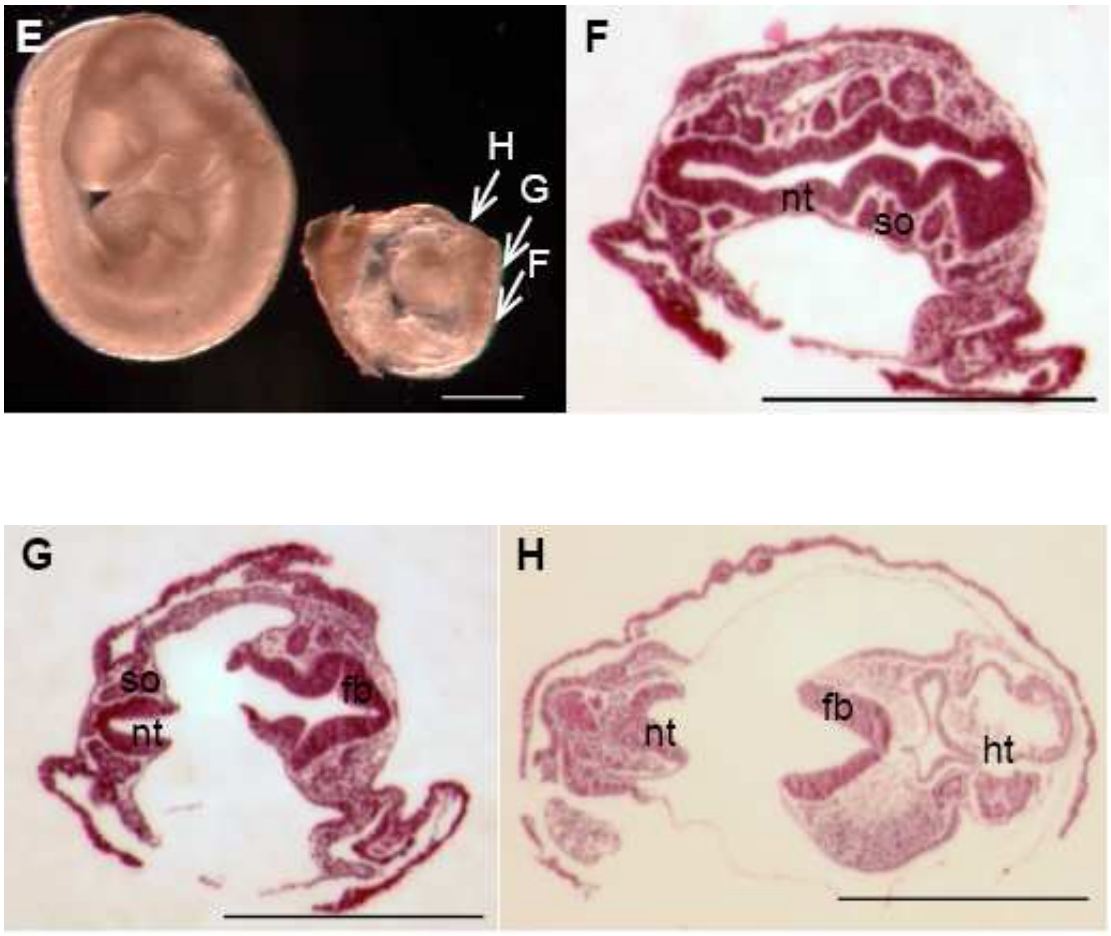
E
H
G
F
F
nt
so
G
so
nt
fb
H
nt
fb
ht

Figure 2.6 Whole mount *in situ* hybridization of *Cyfip1*$^{Gt/Gt}$ mutant embryos.

Upper panel: *T* gene expression in two w.t. embryos (left) and a presumed *Cyfip1*$^{Gt/Gt}$ mutant embryo (right) at 8.5dpc. In the *Cyfip1*$^{Gt/Gt}$ embryo, the T gene probe shows strong expression in the notochord. The expression pattern is the same as it shows in the wild-type embryos. Lower panel: *Fgf8* expression in a presumed *Cyfip1*$^{Gt/Gt}$ mutant embryo and its w.t. littermate at 9.5dpc. The *Fgf8* probe detected widely expression in the wild-type embryo, especially in the central nervous system and heart region, whereas the expression of *Fgf8* is very low, if there is any, in the *Cyfip1*$^{Gt/Gt}$ embryo compare to its wild-type littermate at 9.5dpc.

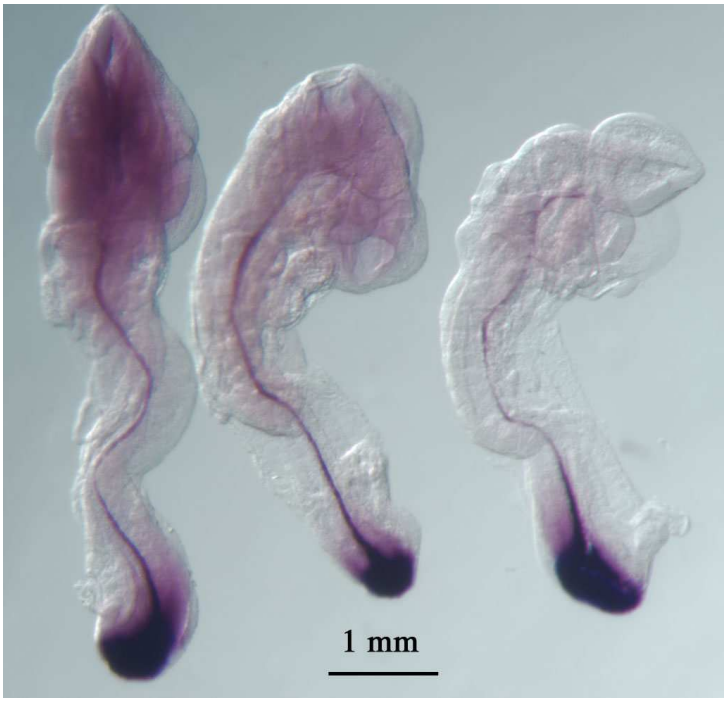
1 mm

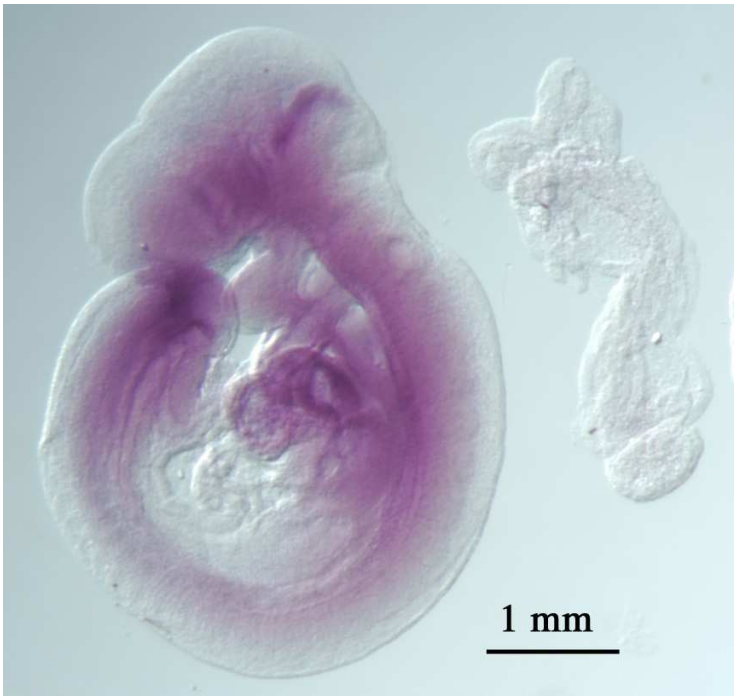
1 mm

CONCLUSION

To gain further understanding of why mice deleted *l7Rl1* die in the early embryonic development, *Cyfip1* is chosen as the first candidate gene among the four genes mapped to the *l7Rl1* locus. *Cyfip1* belongs to a highly conserved gene family and its orthlogs of *Cyfip1* have been studied in different organisms. It has been reported that the losts of function of Cyfip results in embryonic lethality in worm and fly, in which embryonic tissues are able to be formed, but the morphogenesis is abnormal. Furthermore, cells are unable to migrate and neural network fails to be formed (Soto, Qadota et al. 2002; Schenck, Bardoni et al. 2003). Cyfip1 is known to involve in the Rac-1-actin cytoskeleton reorganization pathway, a process essential in cell movement (Schenck, Bardoni et al. 2003; Kobayashi, Kuroda et al. 1998). We hypothesized that *Cyfip1* plays important role in embryogenesis and it is possible that lost of *Cyfip1* function lead to the failure of the early embryonic development.

In order to confirm the XG769 gene-trap ES cell line, we have demonstrated by RT-PCR that the band with 1Kb PCR product was detected by using Shcy12-1F and Shyc18-1R primers in wild type ES. In contrast, one band with 1Kb PCR product and another band with 450bp product expecting from both wild type transcript and gene-trap transcript respectively, were detected by using Shcy12-F, Shyc18-1R and GT-β-reverse primers. Furthermore, in Northern blot analysis, the wild type RNA showed one band with 4Kb in size, while one similar size band and addition one larger size band were detected in heterozygous *Cyfip1*$^{Gt/+}$ RNA sample.

We have generated *Cyfip1*$^{Gt/+}$ mice from a *Cyfip1* gene-trap ES cell line. Heterozygous *Cyfip1*$^{Gt/+}$ mice were normal and fertile, however, *Cyfip1*$^{Gt/Gt}$ is embryonic lethal, as we expected, however, the embryos could survive at the peri-implantation stage since no resorbing moles were observed at 8.5dpc. The heterozygous *Cyfip1*$^{Gt/+}$ intercrossing agreed with the Mendel's law that about 25% of embryos were abnormal suggesting the *Cyfip1*$^{Gt/Gt}$ homozygous genotype at 9.5dpc. Unlike the phenotype observed homologous *l7Rl1* deletion, the mutant embryos proceeded through gastrulation and started to show developmental arrest around 8.5dpc. *Cyfip1*$^{Gt/Gt}$ had only 6-12 somites at 9.5dpc, equivalent to the normal embryos at 8.5dpc. Thus, the peri-implantation lethality in *l7Rl1* deletion is not a resulting of missing only *Cyfip1* gene, however, it is still possible the phenotype of the deletion of *l7Rl1* locus might result from the combination of multiple genes including *Cyfip1*.

CHAPTER III

CHARACTERIZATION OF THE TWO ENU-INDUCED MUTATIONS

INTRODUCTION

l7Rl1, a locus close and proximal to the pink-eyed dilution gene in mouse chromosome 7, is required for peri-implantation survival in the mouse (Russell, Montgomery et al. 1995; Wu, Rinchik et al. 2000). The critical region of *l7Rl1* has been defined by deletion/physical mapping and complementation analysis and is 300kb in overall size (Wu, Rinchik et al. 2000). In a project to use the *p*-deletion mutations to recover ENU induced mutations, two independent recessive-lethal mutations ,$l7Rl1^{ENU2R}$ and $l7Rl1^{ENU3R}$ were found and further mapped to the critical region of *l7Rl1* (Rinchik, Carpenter et al. 1995). Complementation analysis shows that both mutations belong to the same complementation group and are probably allelic.

The null phenotype of *l7Rl1* has been defined as peri-implantation lethal. Homozygous mutant embryos degenerate between E4.5 and E5.5 (Wu, Rinchik et al. 2000). Previous study suggested that four genes reside at *l7Rl1* locus within the *l7Rl1*critival interval (Chai, Locke et al. 2003),however it remains unclear how any one of these genes contributes to the implantation failure.

In this study, to gain further understanding of the function of the *l7Rl1* locus, we determined whether the prenatal-lethal phenotypes observed in either $l7Rl1^{ENU2R}$ or $l7Rl1^{ENU3R}$ homozygous mutants was similar, or identical to the peri-implantation arrest

in the *l7Rl1* mutant with deletion of the entire four-gene region. The affected gene in the two ENU-induced mutations has also been identified.

MATERIALS AND METHODS

Mice

All animal were bred at the mouse facility at Oak Ridge National Laboratory. The two ENU-induced heterozygote strains $l7Rl1^{ENU2R}$ and $l7Rl1^{ENU3R}$ were generated and maintained as described in the Introduction Chapter; and the gene-trap heterozygote $Cyfip1^{Gt/+}$ were generated as described previously in the Chapter 2. To test if the three mutations were allelic, complementation crosses were performed, in which $l7Rl1^{ENU2R}$ and $l7Rl1^{ENU3R}$ heterozygotes were mated to each other and also mated to $Cyfip1^{Gt/+}$ heterozygotes as well.

Embryo observation and histology

Mice were naturally mated, and the day of the vaginal plug found was considered to be 0.5dpc. Uteri of pregnant females were dissected in 1 x PBS at embryonic days 8.5, 9.5, 10.5 and 11.5. Embryo dissection was followed by the protocol described in Nagy et al., 2003 (Manipulating the Mouse Embryo).

For histological sections, dissected embryos were fixed overnight in ice-cold 4% paraformaldehyde diluted from 16% paraformaldehyde solution (EMS) in PBS, dehydrated through a graded ethanol series and embedded in paraffin, sectioned at 5-7μm, and stained with H&E.

The embryos and sections were photographed using a Zeiss SV11 dissection microscope and Spot 100 digital camera connected to a Macintosh computer.

Total RNA isolation and RT-PCR

21A and D7R75M are the background strains of the two ENU induced mutations *l7Rl1*$^{ENU2R/+}$ and *l7Rl1*$^{ENU3R/+}$. Spleens from *l7Rl1*$^{ENU2R/+}$, *l7Rl1*$^{ENU3R/+}$, 21A and D7R75M mice were obtained and snap-frozen in liquid N_2, and total RNA from different mouse stocks was extracted by the Trizol method following the manufacturer's instructions (Eppendorf-5 prime, Inc. Boulder, CO). cDNA was prepared using Invitrogen's SuperScript® First-Strand Synthesis System with Superscript III reverse transcriptase . The synthesized cDNA was purified using QIAGEN quick PCR purification kit following the manufacturer's instructions and stored at -20°C until required.

Screening of *Cyfip1* transcript

First strand cDNA from the four mouse strains was used directly for PCR with specific primers designed to cover the entire *Cyfip1* transcript in four overlapping amplicons. Primers used for screening can be found in Table 3.1. PCR parameters: 96°C 5 min; 39 cycles of 96°C 30 sec, 55°C 30 sec, 72°C 30sec; 7 2°C 10 min; 4°C hold.

Genomic DNA extraction

Genomic DNA from *l7Rl1*$^{ENU2R/+}$, *l7Rl1*$^{ENU3R/+}$, 21A and D7R75M mice was extracted from mouse spleens following the established protocol. Briefly, the entire spleen was grinded in liquid N_2, digested with proteinease K, extracted with phenol/ chloroform

Table 3.1 Primers and probes used in the study

Primer names	Primer Sequence	Study purposes
Shyc2-1F	5'-AGTGACACTAGAGGACGCACTGT-3'	Screening *Cfyip1* transcript
Shyc11/12-1R	5'-TGTGACTACCTCGCTATTGCTGTA-3'	Screening *Cfyip1* transcript
Shyc9-1F	5'-TCCAAAATCGACAAGTATTTCAAG -3'	Screening *Cfyip1* transcript
Shyc18-1R	5'- TGCCTCAATCTCATCATAGAGAAA -3'	Screening *Cfyip1* transcript
Shyc17-1F	5'- CTGACTGATCACATCCTAGAGACC -3'	Screening *Cfyip1* transcript
Shyc27-1R	5'- TCGAGGTAAGATATTCTGGAAAGG -3'	Screening *Cfyip1* transcript
Shyc25-1F	5'- GTGAAAACTCTGATGGAAGTGATG -3'	Screening *Cfyip1* transcript
Shyc31-1R	5'- TGGCAACAACTAGTAACCGTATTC -3'	Screening *Cfyip1* transcript
Shyc25-1F	5'- GTGAAAACTCTGATGGAAGTGATG -3'	Screening 785DSJ mutant
Shyc27-1R	5'- TCGAGGTAAGATATTCTGGAAAGG -3'	Screening 785DSJ mutant
Shyc3-1F	5'- AGATACATCGAACAAGCAACTGTC -3'	Screening 828DSJ mutant
Shyc-SeqR	5'- GGGGATTACCTTCATTACACTGAC -3'	Screening 828DSJ mutant
Shyc26-1F	5'- ATCCTGGAGTTCTTCCACCAC-3'	Sequencing 785DSJ PCR product
Shyc5/6-SeqR2	5'- TAGCAGGAAGACAAGAAAACAGC -3'	Sequencing 828DJ PCR product
T7 primer	5'-TAATACGACTCACTATAG-3'	Sequencing plasmid DNA
Sp6 primer	5'-ATTTAGGTGACACTATAG-3'	Sequencing plasmid DNA
785DSJ Taqman probe	FAM – CTGCGGGAGTCTTT	Taqman assay
828DSJ Taqman probe	FAM – CCCGAGAGAAATGC	Taqman assay

and precipitated with ethanol. The DNA was dissolved in TE buffer (10mM Tris-Cl pH 7.5 and 1mM ethylenediaminetetraacetic acid [EDTA]) and stored at 4°C.

Screening of *Cyfip1* genomic DNA

Genomic DNA from the four mouse strain was used directly for PCR with specific primers designed to flank the potential mutation region in *Cyfip1* gene. For Screening 785DSJ ($l7Rl1^{ENU2R/+}$ = $Cyfip1^{ENU2R/+}$) mutant, primers Shyc25-1F and Shyc27-1R were used; for screening 828DSJ ($l7Rl1^{ENU3R/+}$ = $Cyfip1^{ENU1R/+}$) mutant, primers Shyc3-1F and Shyc-SeqR were used (Table 3.1). PCR parameters: 96°C 5 min; 39 cycles of 96°C 30 sec, 55°C 30 sec, 72°C 30sec; 72°C 10 min; 4°C hold.

Subclone of the PCR products and DNA sequencing

PCR products were either sequenced directly or cloned into a vector and then sequenced. For the direct sequencing, PCR products were purified by PCR cleaning kit according to the manufacturer's instructions (Qiagen), then sequenced at Vanderbilt University. Shyc26-1F and Shyc5/6-SeqR2 primers (Table3.1) were designed specifically for sequencing of the PCR products from 785DSJ and 828DJ mutant genomic DNA, respectively. Otherwise, a fraction of the above PCR products were subcloned into pCRII-TOPO vector using TOPO TA cloning kit (Invitrogen) following the manufacturer's instructions. At least 6 clones were picked and grown in small culture. Plasmid DNA was purified using Wizard Plus SV mini-prep kit (Promega) for sequencing. Plasmids DNAs were sequenced using SP6 or T7 primers (Table 3.1). Sequences were analyzed using Sequencher v4.0 on a Macintosh G5 computer.

Taqman assay for 785DSJ and 828DSJ

The Cepheid SmartCycler® system was used to detect PCR products using oligonucleotide probes specifically designed for the transcripts of the two ENU-induced mutations. 785DSJ and 828DSJ Taqman probe were designed by the Applied Biosystems (www.AppliedBiosystems.com) Taqman Assays-by-Design service and provided in 20x Taqman Assay mixature followed by submission of the target sequences from the two transcripts. 20x Taqman mix has been ordered from the same company. To perform the Taqman assay, 1.25µl 20x Taqman assay mix, 12.5µl 2x Taqman universal mix (Applied Biosystems), 1µl cDNA were present in each reaction. Both 785DSJ and 828DSJ cDNA samples as well as 21A and 7R75M cDNA were analyzed in triplicates in a final reaction volume of 25µl. PCR amplification included an initial phase of 2 minutes at 50°C, followed by 10 minutes at 95°C, 49 cycles of 15 seconds at 95°C and 1 minute at 60°C.

RESULTS

l7Rl1^{ENU2R} and *l7Rl1*^{ENU3R} homozygous mutant embryos are not peri-implantation lethal

In order to define the phenotype of the two ENU-induced mutations, intercrosses of *l7Rl1*^{ENU2R} heterozygotes and of *l7Rl1*^{ENU3R} heterozygotes were performed and uteri of pregnant females were dissected at 8.5dpc and 9.5dpc. In the total number of 118, only approximately 3% empty deciduas were observed, indicating that homozygous embryos were able to survive through the embryonic day 5.5. Thus, *l7Rl1*^{ENU2R} and *l7Rl1*^{ENU3R}

homozygous mutant embryos were different from the peri-implantation lethality phenotype of homozygous deletion of the *l7Rl1* genomic region.

l7Rl1^{ENU2R} and *l7Rl1*^{ENU3R} homozygous mutant embryos show developmental arrest around 8.5dpc

In order to further define the mutant phenotype of the two ENU-induced mutations, embryos from the two experimental intercross mating (+ p^{7R}/*m p x*; + p^{7R}/*m p*) were dissected and examined at 8.5dpc, 9.5dpc and 10.5dpc. Histological sections were examined for 9.5dpc mutant embryos. + P^{7R}/+ p^{7R} mice were mated as the control group. At 9.5dpc, a total of 60 (785DSJ) and 103 (828DSJ) decidua from the two experimental mating was observed. 12 out of 60 (21.6%) and 23 out of 103 (22.3%) were developmentally abnormal embryos, as compared with no abnormal embryos but one empty decidua found from a total of thirty-two 9.5dpc embryos examined in the control group (Table 3.2). According to Mendelian rule, 25% of the offspring should be homozygotes in a heterozygous intercross; thus, we conclude that about ¼ abnormal embryos observed in the experimental mating were the homozygous ENU-induced mutations.

The morphology of the wild-type embryo and presumed *l7Rl1*^{ENU2R} / *l7Rl1*^{ENU2R} and *l7Rl1*^{ENU3R} / *l7Rl1*^{ENU3R} mutant embryos was shown in Figure 3.1 and Figure 3.2. Both *l7Rl1*^{ENU2R} and *l7Rl1*^{ENU3R} mutation homozygotes displayed similar lethal phenotypes: embryos were able to implant and subsequently developed normally until 7.5-8.5dpc, at which time the anterior-posterior axis of the mutant embryos could not be elongated further and the mutant embryos remained in lordotic position. At 9.5dpc, the

Table 3.2 Intercross mating of ENU-induced mutants

	Intercross mating	Observed decidua	Number of abnormal embryo (percentage)
Control	+ P^{7R}/+ p x + P^{7R}/+ p	32	0 (1 empty decidua)
Experiment 1[A]	+ P^{7R}/m p x + P^{7R}/m p	60	12/60 (21.6%)
Experiment 2[B]	+ P^{7R}/m p x + P^{7R}/m p	103	23/103 (22.3%)

A: 785DSJ x 785DSJ (*l7Rl1*^{ENU2R} x *l7Rl1*^{ENU2R})

B: 828DSJ x 828DSJ (*l7Rl1*^{ENU3R} x *l7Rl1*^{ENU3R})

Figure 3.1 The embryo morphology in wild-type and *l7Rl1*^{ENU2R} and *l7Rl1*^{ENU3R} homologous mutants

A: ventral view of a normal (wild-type [w.t.]) 8-somite stage (~8.5dpc) embryo. The developing neural tube is runs linearly up the midline of the embryo with somites pair on eitherside. C and E: dorsal view of 9.5dpc *l7Rl1*^{ENU3R} / *l7Rl1*^{ENU3R} and *l7Rl1*^{ENU2R} / *l7Rl1*^{ENU2R} mutant embryos, respectively. The neural tube and the developing brain were kinky, and somites were visible but appeared disorganized. G: littermates at 9.5dpc from an intercross of mutation carriers from stock 785DSJ (+ / *l7Rl1*^{ENU2R} x + / *l7Rl1*^{ENU2R}). The amnion membrane was removed from the left and the middle embryos. The embryo on the left appeared normal although its developmental stage was delayed compare to other w.t. littlemates (not shown), which is a common phenomenon at this developmental stage. The middle and the right embryos displayed kinky neural tubes, wavy developing brain, and disorganized somite pairs. Arrows: neural tube. Arrowheads: somites. Scale bars: 0.5mm.

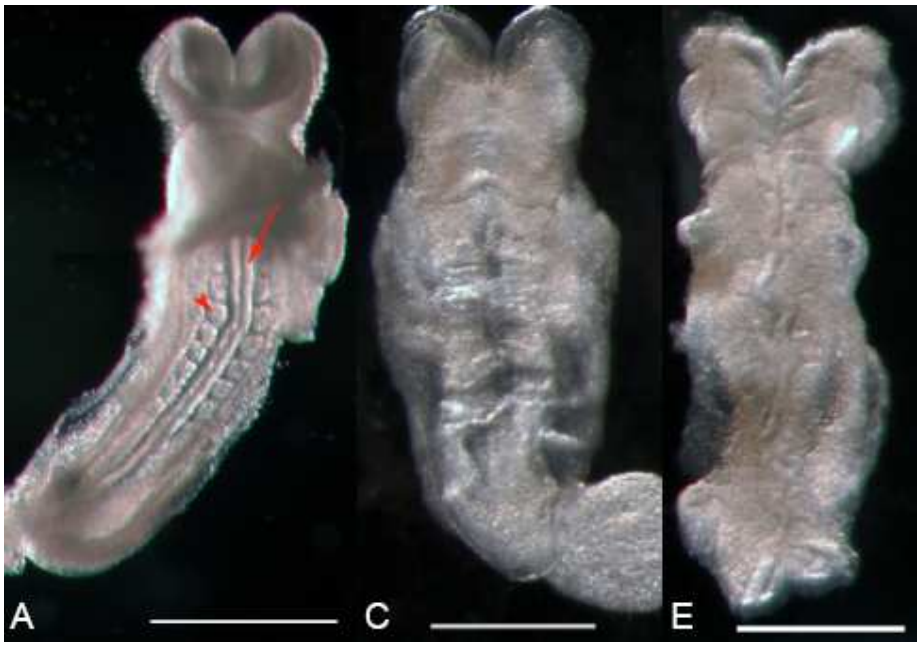
A
C
E


G

Figure 3. 2 Histological section of wild-type and *l7Rl1*^{ENU2R} / *l7Rl1*^{ENU2R} embryos

A: a wild-type (left) and a mutant (right) 9.0dpc embryos from a intercross of stock 785DSJ (+ / *l7Rl1*^{ENU2R} x + / *l7Rl1*^{ENU2R}). Arrows and letters B, C and D indicate the section plans for the panels B-D. B: Section of the wild-type embryo illustrates the smooth neural tube (nt) and flanking somites (so). C: Section of the *l7Rl1*^{ENU2R} / *l7Rl1*^{ENU2R} mutant embryo through the trunk region. The kinky neural tube and disorganized somites are evident and the primitive heart tissue and the first brachial arch (ba) are formed. D: Section of the *l7Rl1*^{ENU2R} / *l7Rl1*^{ENU2R} mutant embryo near the head showed wavy forebrain (fb).

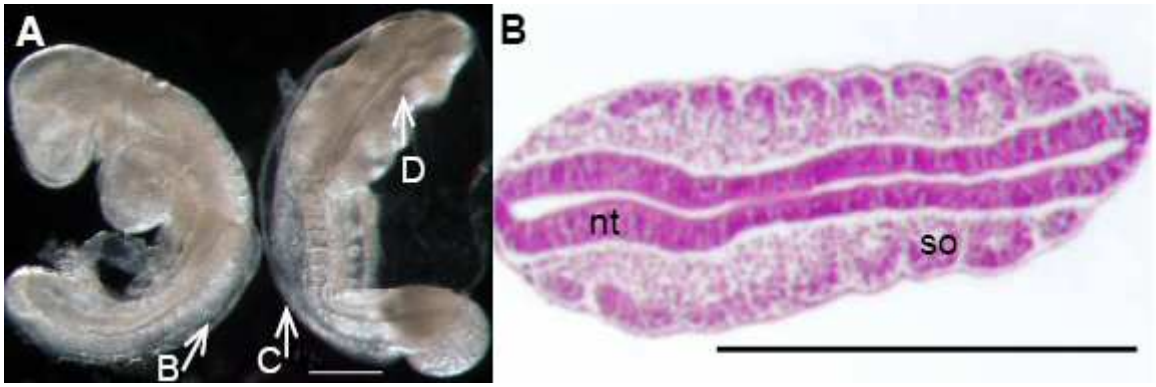
A
D
B
C
B
nt
so

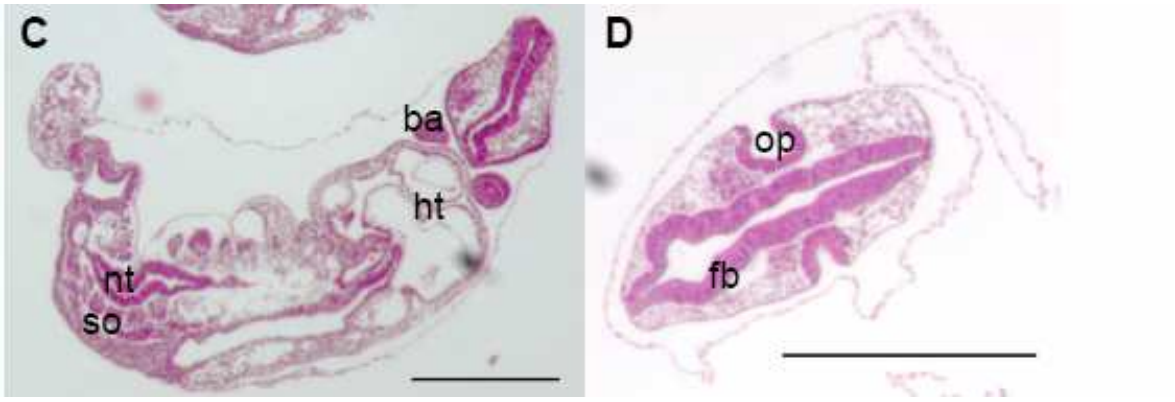
C
ba
ht
nt
so
D
op
fb

mutant embryos usually had 6-12 somites and displayed abnormalities in the neural tube. Normally straight neural tubes became kinky, and similar defects were also observed in developing brain. Neural tube closure was rarely observed in the mutant embryos by 9.5dpc. Somites were developed, albeit disorganized, as evident in the section of the mutant embryos. Primitive cardiac structure was initiated, but its development was arrested around 8.5dpc. Mutant embryos disintegrated after 10.5dpc.

In conclusion, these results suggested that both ENU alleles have identical effects on arresting development. In addition, the embryo abnormality caused by the ENU mutation occurs significantly later than peri-implantation arrest in the multi-gene deletion at *l7Rl1* locus.

Of particular note was that the abnormal developmental phenotype observed in these two ENU-induced mutations was identical to that observed for the $Cyfip1^{Gt/Gt}$ homozygous embryos in 8.5 to 10.5dpc. Thus, the two ENU-induced mutations are very likely alleles of *Cyfip1*, known to map into the same critical region.

The two ENU-induced mutations and the *Cyfip1* gene-trap mutation are allelic

$l7Rl1^{ENU2R}$ and $l7Rl1^{ENU3R}$ heterozygotes ENU-induced mutants were mated each other or mated to $Cyfip1^{Gt/+}$. Embryonic analysis of the compound heterozygotes from all possible combinations showed the same phenotype as we observed in homozygotes embryos in all three mutations (Figure 3.3): embryonic development arrest, failure in anterior-posterior axis elongation and abnormal development in neural tube and brain. Thus, both the complementation analyses and the similarity/identity in the lethal-

Figure 3.3 Image of mutant embryos from complementation tests

A: Dorsal view of a compound heterozygous mutant embryo from cross of *Cyfip1*$^{Gt/+}$ and *Cyfip1*$^{ENUR1/+}$ at 9.5dpc. The deformed neural tube and brain were prominent. The mutant embryo developed somites (not clear in this image), but displayed kinky neural tube. B: A mutant embryo from cross of *Cyfip1*$^{ENUR2/+}$ and *Cyfip1*$^{ENUR1/+}$ at 9.5dpc. The mutant embryo arrested at 8.5dpc stage. The yolk sac was developed and still intact. The wavy neural tube was clearly visible in the hindgut pocket region, flanked with somite pairs. Arrows: neural tube. Arrowheads: somites. Scale bars: 0.5mm.

A

B

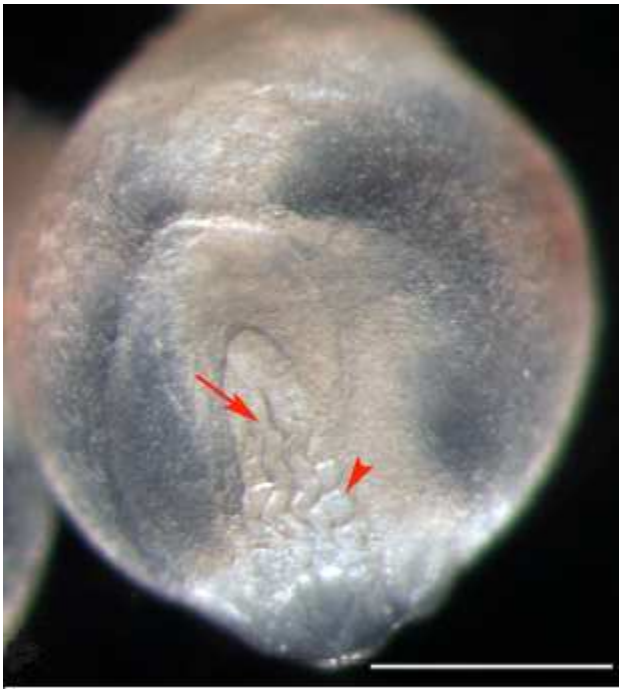

phenotype analyses suggested that ENU-induced *l7Rl1*^{ENU2R} and *l7Rl1*^{ENU3R} should be investigated as *Cyfip1* mutations.

Characterization of mutant transcripts of *Cyfip1*^{ENU1R} and *Cyfip1*^{ENU2R}

Genetic analysis suggested that two ENU-induced mutations could be alleles of *Cyfip1*. ENU is a known supermutagen that most often causes single-base changes at genomic DNA level and leads to abnormal or absent transcripts in mice. Most ENU-induced mutations are missense mutations, followed by splice site and nonsense mutations, and some can lead to cryptic transcripts. In order to identify mutant transcripts directly, cDNA was synthesized from the spleens of *l7Rl1*^{ENU2R} and *l7Rl1*^{ENU3R} mutants. PCR primers were designed so that four overlapping amplicons cover the entire *Cyfip1* transcript (4325 bp in length with 31 exons, based on Ensembl gene ID ENSMUSG00000030447) (Chai, Locke et al. 2003)(Figure 3.4). All four PCR amplicons amplified from cDNA were first assayed on 0.8% agarose gels to ensure that PCR product sizes match those predicted. Then the PCR products were directly sequenced using the same PCR primers. Sequence analysis indicated that two amplicons, amplified by primers Shyc25-1F and Shyc31-1R from *Cyfip1*$^{ENU1R/+}$ cDNA and by primers Shyc2-1F and Shyc11/12-1R from *Cyfip1*$^{ENU2R/+}$ cDNA, gave only partially readable signals, unlike all other direct sequencing results. Therefore, we cloned these two PCR amplicons into pCRII-TOPO vector and at least 6 clones from each amplicon were randomly selected for sequencing from both ends. *l7Rl1*^{ENU2R} and *l7Rl1*^{ENU3R} were generated by treat the mouse strain 21A with ENU and newly recovered ENU-induced mutations were maintained by

Figure 3.4 Characterization of mutant transcripts of *Cyfip1*^{ENU1R} and *Cyfip1*^{ENU2R}

Cyfip1 transcript and its amino acid translation based on Chai et al, 2003. All primer sequences used for PCR amplification of *Cyfip1* transcripts, as well as for sequencing, to screen and identify the altered transcripts in *Cyfip1*^{ENU1R} and *Cyfip1*^{ENU2R} mutations, are indicated at appropriate locations above the sequence. The nucleotides along with the corresponding amino acids that are deleted in the mutant transcripts from *Cyfip1*^{ENU1R} and *Cyfip1*^{ENU2R} alleles are highlighted in grey boxes.

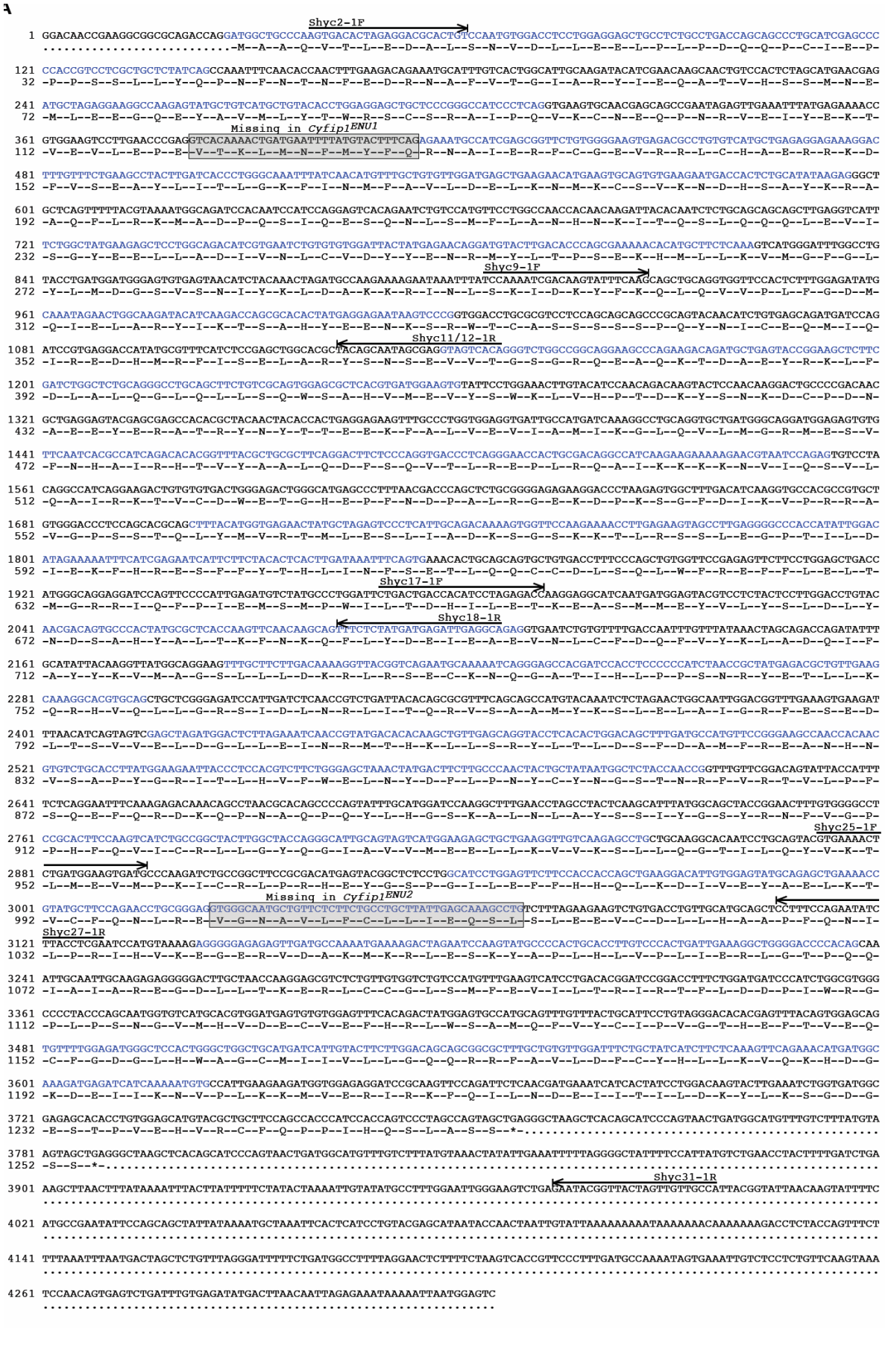
A
Shyc2-1F
Missing in Cyfip1ENU1
Shyc9-1F
Shyc11/12-1R
Shyc17-1F
Shyc18-1R
Shyc25-1F
Missing in Cyfip1ENU2
Shyc27-1R
Shyc31-1R

crossing heterozygotes to D7R75M. Sequence analysis indicated that 45 bp was missing from the end of the exon27 in the 21A allele of the *Cyfip1* transcript in 785DSJ heterozygotes (identifying the *Cyfip1*^{ENU2R} *p* haplotype), and 33 bp was missing from the end of exon 5 of *Cyfip1*$^{ENU1R/+}$ in the 21A allele of the *Cyfip1* transcript in 828DSJ heterozygotes (identifying the Cyfip1^{ENUR} *p* haplotype) (Figure 3.4). On the other hand, the D7R75M transcripts (corresponding to the + p^{7R} haplotype) aligned to the reference *Cyfip1* transcript. The 21A and D7R75M transcripts were differentiated based on the single nucleotide polymorphism (SNP) within the sequenced regions (data not shown). The mutant transcripts from alleles *Cyfip1*^{ENU1R} and *Cyfip1*^{ENU2R} can be translated into mutant proteins with removal of 11 and 15 amino acids near the N- and C-terminal of the Cyfip1 protein, respectively. As an additional control, all four amplicons were also amplified from cDNA prepared from total RNA from stocks 21A (+ *p* / + *p*) and D7R75M (+ p^{7R} / + p^{7R}), and the RT-PCR products were directly sequenced. No cryptic transcript was identified in either RNA preparation, confirming that ENU mutagenesis generated *Cyfip1*^{ENU1R} and *Cyfip1*^{ENU2R} mutant transcripts, and that the observed aberrant sequencing results were not the results of a simple SNP(s) between the 21A and 7R75M.

Identification of genomic lesions of *Cyfip1*^{ENU1R} and *Cyfip1*^{ENU2R} mutations

The identification of two cryptic *Cyfip1* transcripts in *Cyfip1*^{ENU1R} and *Cyfip1*^{ENU2R} mutations indicated specific regions of the *Cyfip1* gene to screen for ENU-induced genomic lesions. PCR primers were designed, of which two primers (Shyc3-1F and Shyc-SeqR) bracketed the *Cyfip1*^{ENU1R} exon 5; two additional primers (Shyc25-1F and Shyc27-1R) bracketed exon 27 in *Cyfip1*^{ENU2R}. Corresponding PCRs were performed

from genomic DNA isolated from mutation carriers (*Cyfip1*^{ENU1R} *p* / + *p*^{7R} and *Cyfip1*^{ENU2R} *p* / + *p*^{7R}), along with genomic DNA from stocks 21A, D7R75M, and 7R75M. These latter background controls were carried out because the mutation carriers (*e.g*, *Cyfip1*^{ENU1R} *p* / + p^{7R}) are not inbred, and so it is necessary to sequence DNA 21A, in which the ENU-induced mutations originated, as well as D7R75M and 7R75M, the two related mouse lines (+ *p*^{7R} / + *p*^{7R}) used to maintain the mutations. Purified PCR products were sequenced directly with the same and also additional primers (Shyc-26-F for *Cyfip1*^{ENU2R} and Shyc5/6-SeqR2 for *Cyfip1*^{ENU1R}). As expected, comparison of DNA sequences detected several SNPs between stock 21A (+ *p* /+ *p*), mutation carriers (e.g., *Cyfip1*^{ENU1R} *p* / *p*^{7R} +), and stock D7R75M (+ *p*^{7R}/+ *p*^{7R}). However, there was one unique one base pair difference, in the mutation carriers of *Cyfip1*$^{ENU1R/+}$ from stock 828DSJ (exon 5) and in the mutation carriers of *Cyfip1*^{ENU2R} from stock 785DSJ (exon 27), respectively, that could not be explained by SNPs among the 21A, D7R75M and 7R75M genomic sequences. Consequently, these two SNPs, a T in *Cyfip1*^{ENU1R} exon 5 replacing a conserved G in the 21A and D7R75M genes, and a T in *Cyfip1*^{ENU2R} exon 27 replacing a conserved C in 21A and D7R75M (see Figure 3.5), must have arisen from ENU treatment. Both the G to T change in the *Cyfip1*^{ENU1R} (828DSJ) allele and the C to T change in *Cyfip1*^{ENU2R} (785DSJ) allele lead to alteration of splice sites leading to the deletion of partial exons and the mutant *Cyfip1* transcripts (Figure 3.4).

Taqman assay for *Cyfip1*^{ENU2R} and *Cyfip1*^{ENU1R}

In order to show direct evidence that the two cryptic transcripts are only exist in each of the ENU-induced mutant carrier, Taqman assay probes were designed to span the

Figure 3.5 Genomic lesions of *Cyfip1*^{ENU1R} and *Cyfip1*^{ENU2R} mutations

A**:** Sequence traces of genomic DNA isolated from *Cyfip1*$^{ENU1R/+}$ heterozygotes. The arrows indicate the ENU-induced point mutation: A G-to-T substitutions for *Cyfip1*^{ENU1R}. The nucleotides within the boxes are deleted in the corresponding mutant transcripts. The vertical line marks the exon-intron boarders.

B: Sequence traces of genomic DNA isolated from +/*Cyfip1*^{ENU2R} heterozygotes. The arrows indicate the ENU-induced point mutations: A C-to-T substitutions for *Cyfip1*^{ENU2R}. The nucleotides within the boxes are deleted in the corresponding mutant transcripts. The vertical line marks the exon-intron boarders.

A

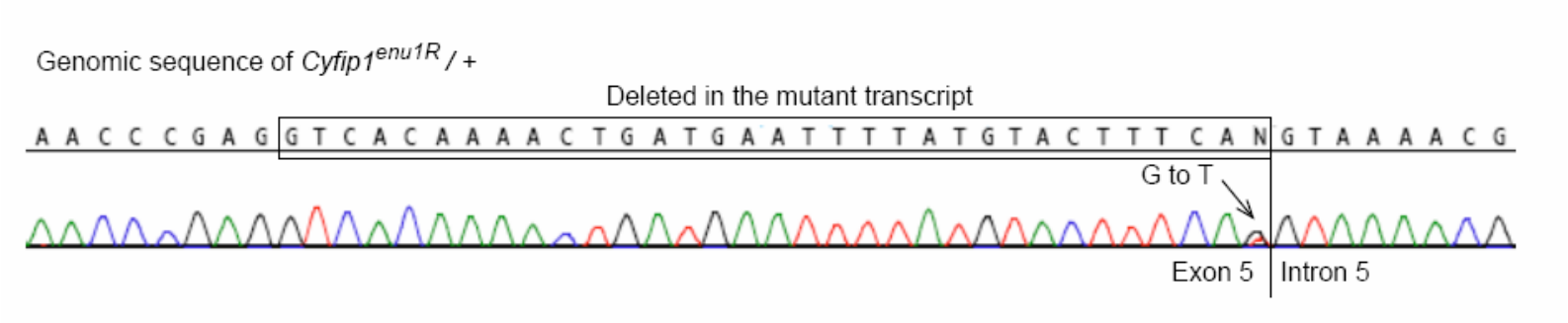
Genomic sequence of Cyfip1enu1R / +
Deleted in the mutant transcript
A A C C C G A G G T C A C A A A A C T G A T G A A T T T T A T G T A C T T T C A N G T A A A A C G
G to T
Exon 5
Intron 5

B

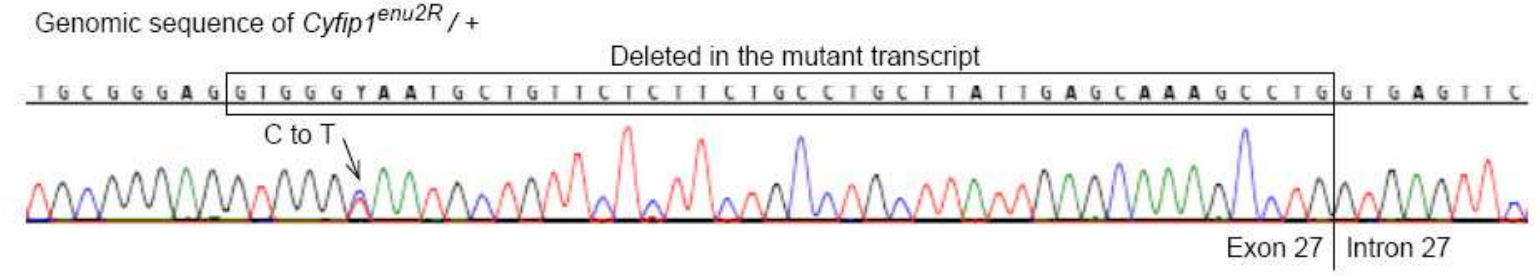
Genomic sequence of Cyfip1enu2R / +
Deleted in the mutant transcript
C to T
Exon 27
Intron 27

missing region of each mutant transcript and cDNA sample synthesized from *Cyfip1*$^{ENU2R/+}$ *Cyfip1*$^{ENU1R/+}$, 21A and 7R75M spleen total RNA were used as template for the real time PCR. Probe of each transcript only generated signal from its corresponding ENU-induced strain, nothing was detected in the two wild-type back ground strain. The results further confirmed the existence of the mutant transcripts in the two ENU-induce mutation, and that the single nucleotide substitutions found in genomic DNA of the two ENU-induced mutations resulting the in-frame exon skipping of the last 33 bp of exon 5 and/or the last 45 bp of exon 27.

CONCLUSION

The *l7Rl1* genomic region is indispensable for embryonic development (Wu, Rinchik et al. 2000). Study the ENU-induced mutations in this region has a great advantage for understanding the genetic contribution of *l7Rl1* genomic region to the embryonic development. Homozygous deletion mutant embryos of *l7Rl1* region degenerate between E4.5 and E5.5 and lead to peri-implantation lethality (Wu, Rinchik et al. 2000). However, two ENU-induced mutation *l7Rl1*^{ENU2R} and *l7Rl1*^{ENU3R} defined in *l7Rl1* region showed a different phenotype in this study. First, only 3% of empty decidua was observed at dpc8.5 from the embryo of heterozygotes inbreeding of *l7Rl1*^{ENU2R} and *l7Rl1*^{ENU3R} mutants, suggesting it is unlikely these two mutants have the same allelic effect as *l7Rl1* region. Second, presumed *l7Rl1*^{ENU2R} / *l7Rl1*^{ENU2R} and *l7Rl1*^{ENU3R} / *l7Rl1*^{ENU3R} mutant embryos showed normal implantation and normal development till 7.5dpc, but abnormal elongation of anterior-posterior and abnormal development of

neural tub at 9.5dpc (Figure 3.1 and 3.2). The similar phenotype of these two mutants also suggested they are allelic. Furthermore, intercross among *l7Rl1*^{ENU2R} and ^{l7Rl1ENU3R} heterozygotes, or *Cyfip1*$^{Gt/+}$ confirmed that the ENU-induced mutations cause the same phenotype as homozygosity for the *Cyfip1* gene trap. Sequencing of the *Cyfip1* transcripts from the ENU mutations confirmed allelism. This result further support the previous conclusion about the gene-trap mutant of *Cyfip1*: dysfunction of *Cyfip1* does not resulting the peri-implantation lethality seen in *l7Rl1* null embryos.

Cyfip1 is highly conserved among different species, although no functional domains of the protein have been identified. Understanding the genetic mechanisms of ENU-enduced mutation will help dissect the functional domains of this gene. Sequence analysis on the mutant transcripts suggested a deletion of 45bp and 33bp in exon 27 and exon 5 of *Cyfip1* gene in the two ENU-induced mutations respectively, which lead to a removal of 11 and 15 amino acids of Cyfip1 protein. ENU-induced mutation usually causes single-base changes at DNA level. ENU mutation could cause point mutation lead to generation of premature proteins due to stop codon, splice donor/acceptor site mutation, and single amino acid alteration (Wienholds, van Eeden et al. 2003; Fossett, Arbour-Reily et al. 1990). Further sequence analysis has dissected two SNPs, which G (wild type) was replaced by T in *Cyfip1*^{ENU1R} exon 5 and C (wild type) was replaced by T in *Cyfip1*^{ENU2R} exon 27. The alteration of single nucleotide led to the use of cryptic splice sites with in-frame exon skipping of the exon 5 or exon 27 (Figure 3.5). ENU-induced mutation lead to alteration of splice site has been reported in Drosophila, zebrafish, mouse, and other organisms (Wienholds, van Eeden et al. 2003; Fossett, Arbour-Reily et

al. 1990). In our case, both *Cyfip1*^{ENU1R} and *Cyfip1*^{ENU2R} mutation lead to splice site alteration and deletion of amino acid fragments. Homolog analysis suggested these two regions are well conserved in different organisms (Figure 3.6). It is clear these two protein regions are essential for the protein function. The conservation of Cyfip1 in different species is manifested almost throughout the entire protein, which suggests the existence of numerous functional and/or structurally indispensable domains within the protein. The lethality of homozygous *Cyfip1*$^{ENU1R/ENU1R}$ and *Cyfip1*$^{ENU2R/ENU2R}$ embryos further suggests that the structurally intact of Cyfip1 protein is required for biological function in *vivo* and is indispensable during mouse embryonic development.

Figure 3.6 Amino Acid missed in two ENU-induced mutations are highly conserved among different organism

Cyfip1^{enu1R} misses AA from #119 ~#129

115 L E P E V T K L M N F M Y F Q R N A I E R F C G E V R R L C H A - E R R K D F V Mouse (AF072697)
115 L E P E V T K L M K F M Y F Q R K A I E R F C S E V K R L C H A - E R R K D F V cyfip2-Human (BC011762)
115 L K P E V S K L G S F M R F T L T A I Q R F C E E V R R L C H S - E K R R D F V Caenorhabditis (AB073209)
115 L E P E V T K L M K F M Y F Q R K A I E R F C S E V K R L C H A - E R R K D F V cyfip2-mouse (AF334144)
115 L A P E V N K L L N F M Y F Q R K A I E A F S G E V K R L C H A - E K R K D F V Drosophila (AAG61254)
115 L E P E V T K L M N F M Y F Q R N A I E R F C G E V R R L C H A - E R R K D F V Human (AAW51477)
115 L E P E V T K L M N F M Y F Q R N A T E R F C A E V K R L C H A - E R R K D F V Xenopus (AAH77907)
115 L E P E V N K L M N F M Y F Q R T A I D R F C G E V R R L C H A - E R R K D F V Zebra-fish (NP_997924)
116 L E P E I K K L K D F M Y F Q K D T I K L F C D H I K K L A S T Y D K K K E T I Dictyostelium (AAR89379)
110 L D L E M S R L R E I Q R W Q S S A S A K L A A D M Q R F S R P - E R R I N - - Arabidopsis (AAT71307)

Cyfip1^{enu2R} misses AA from #1000 ~#1014

970 P G I L E F F H H Q L K D I A E Y A E L K T V C F Q N L R E V G N A V L F C L L Mouse (AF072697)
969 P G I L E F F H H Q L K D I I E Y A E L K T D V F Q S L R E V G N A I L F C L L cyfip2-Human (BC011762)
973 N A L L Q Y Y V H H L E A V G K Y P E L K S E F C Q D L R E L G N M I V F C Q Q Caenorhabditis (AB073209)
969 P G I L E F F H H Q L K D I I E Y A E L K T D V F Q S L R E V G N A I L F C L L cyfip2-mouse (AF334144)
992 P G V L S Y Y Q A H L T D I V Q Y P D A K T E L F Q S F R E F G N S I I F C L L Drosophila (AAG61254)
970 P G I L E F F H H Q L K D I V E Y A E L K T V C F Q N L R E V G N A I L F C L L Human (AAW51477)
970 P G I L E F F H H Q L K D I V E Y A E L K S V C F Q N L R E V G N A L L F C L L Zebra-fish (NP_997924)
964 E G G Y G Y F Q L K L K D I Y I Y P D L R P E V L Q T F R E L G N S L V F M NL Dictyostelium (AAR89379)
978 T G C M K L I R E Q L N W G T K - S E L K S E V L R G I K E I G S V I Y T M G L Arabidopsis (AAT71307)

1010 I E Q S L S L E E V C D L L H A A P F Q N I L P R I H V K E G E R V D A K M K R Mouse (AF072697)
1009 I E Q A L S Q E E V C D L L H A A P F Q N I L P R V Y I K E G E R L E V R M K R cyfip2-Human (BC011762)
1013 L E V A L G Q E E A H D L F L A A A Y T G T V P Q P P A R N A Q E Q M K Q L A K Caenorhabditis (AB073209)
1009 I E Q A L S Q E E V C D L L H A A P F Q N I L P R V Y I K E G E R L E V R M K R cyfip2-mouse (AF334144)
1032 I E Q A L S Q E E V C D L L H A A L F Q N I F P R P F C K E N E K P E A K Q K R Drosophila (AAG61254)
1010 I E Q S L S L E E V C D L L H A A P F Q N I L P R V H V K E G E R L D A K M K R Human (AAW51477)
1010 T E Q S L S Q E E V C D L L H A A P F Q N I L P R V H V K E G E R L D A K M K R Zebra-fish (NP_997924)
1004 L D Q V I T Q T D S Y N F A K A A P F L G I T P E T W - K D L E P S T E D P T L Dictyostelium (AAR89379
1017 L D I V L R E V D T K R F M Q T A P W L G L I P G A E G Q I V N A Q D G E S P L Arabidopsis (AAT71307)

CHAPTER IV

SUMMARY AND DISCUSSION

In this study, we have experimentally demonstrated that *Cyfip1* is required for embryonic development beyond 8.5dpc, but loss of the gene function does not cause the peri-implantation lethality associated with *l7Rl1*. We have generated heterozygous *Cyfip1*$^{Gt/+}$ chimeric mice from the gene-trap ES cell clone, and have produced homozygous *Cyfip1*$^{Gt/Gt}$ embryos and characterized the phenotype. Homozygous *Cyfip1* mutant embryos displayed embryonic development arrest at around 8.5dpc and showed defects in the central nervous system.

Clinical data indicate that a significant portion of early miscarriage is caused by genetic defects (Alberman and Creasy 1977; Goddijn and Leschot 2000). Therefore, identification of a gene(s) in the *l7Rl1* locus that causes the peri-implantation lethality may provide insight into a molecular mechanism of early miscarriage. There are four genes located in the *l7Rl1* locus lost of which may cause the peri-implantation lethality: *Tubgcp5*, *Cyfip1*, *Nipa2*, and *Nipa1*. At least three of them, *Tubgcp5*, *Cyfip1*, and *Nipa2* genes are expressed in the ES cell in that their gene trap lines have been generated (International Gene Trap Consortium, http://www.genetrap.org). Since the null mutation of *Cyfip1* causes early embryo lethality in worm and fly (Soto, Qadota et al. 2002; Schenck, Bardoni et al. 2003) and the gene is known in the Rac1 – actin cytoskeleton reorganization pathway in the cell (Hall 1998), a process essential in cell movement, We hypothesized that *Cyfip1* is a candidate for the peri-implantation lethal in the *l7Rl1* locus.

By using histology analysis and RNA whole mount *in situ* hybridization, the phenotype of *Cyfip1*$^{Gt/Gt}$ embryos, obtained from the intercross of transgenic mouse of *Cyfip1*$^{Gt/+}$ has been studied. We have shown that *Cyfip1*$^{Gt/Gt}$ is embryonic lethal and has severe defects in the development of the central nervous system. To further characterize and understand the mutant phenotype in the central nervous system, FISH analysis using specific probes targeting central nervous system can be performed for highlighting the affected organs and providing more detailed information.

Second, we have analyzed the homozygous phenotype of two ENU-induced mutants, 785DSJ (*l7Rl1*$^{ENU2R/+}$=*Cyfip1*$^{ENU2R/+}$) and 828DSJ (*l7Rl1*$^{ENU3R/+}$=*Cyfip1*$^{ENU1R/+}$). The phenotype of these two mutants was identical to that observed in *Cyfip1*$^{Gt/Gt}$ homozygotes, which was embryonic lethal at 8.5- to 10.5-dpc. I have demonstrated that the two ENU-induced mutations are alleles of *Cyfip1*. We have further characterized the genetic alterations of the two ENU mutations. Sequence analysis revealed that one point mutation caused a C to T change in 785DSJ leading 45bp missing in the transcript at the end of exon 27; and one point mutation caused a G to T change in 828DSJ leading 33bp missing in the transcript at the end of exon 5. The existence of the two cryptic transcripts has been confirmed by Taqman assay using probes span the missing region of each mutant transcript.

Based on the sequence analysis of the transcripts in the ENU-induced mutations, the partial deletion of the two exons will ultimately lead to a removal of 11 amino acids at the position 119-129 near the N-terminal and 15 amino acids at the position 1000-1014 near the C-terminal of the Cyfip1 protein, which consists 1253 amino acid. Homologous analysis showed that these two deletion regions are highly conserved at the protein level

in different organisms, but no functional domain or motif has been identified for the Cyfip proteins based on the reference mRNA sequence. Taking the fact that *Cyfip1*^{ENU1R} and *Cyfip1*^{ENU2R} mutations suffered similar lethal phenotype as the *Cyfip1*$^{Gt/Gt}$, which has lost more than 2/3 of the entire coding sequence, we concluded that both N- and C-terminal regions of the protein are important for its *in vivo* biological function during the embryogenesis. We have demonstrated the existence of three mutant transcripts by RT-PCR and Northern analysis. Further study of the mutated Cyfip1 protein will be generating an antibody targeting the residue region of the truncated Cyfip1 protein, and detecting the protein by immunohistochemistry.

Third, three mouse *Cyfip1* mutations reported in my study including one gene-trap null mutant and two ENU mutants showed similar embryonic lethal phenotype: mutant embryos proceeded through gastrulation and formed three germ layers. They developed neural tube, heart, somite pairs and extraembryonic tissues. However, in the early organogenesis, the neural tube was kinky, somites appeared disorganized, and heart development was arrested at early stage. Thus the lethal phenotype of the *Cyfip1* mutations in mice was consistent with *Cyfip* mutations in other multicellular organisms. For example, for null mutations of *Cyfip* in worm and fly, embryonic tissues are formed, but their morphogenesis is abnormal. Cells in the null mutant are unable to migrate and fail to form neural network (Soto, Qadota et al. 2002; Schenck, Bardoni et al. 2003). The generation of the *Cyfip1* gene-trap ES cell line indicates that this gene is expressed at ES cell stage, ~ 3.5 dpc mouse embryos. Later at ~8.5 dpc, the *Cyfip1* is highly expressed in the developing neural tube (Koster, Schinke et al. 1998), which was consistent with the onset of wavy neural tube in the *Cyfip1* mutants. Since the development of the mutant

embryos was in general arrested from 8.5 dpc and onward, all tissues appeared to be affected by the *Cyfip1* mutations.

Fourth, the phenotype of the deletion of *Cyfip1* is different from the peri-implantation phenotype observed in *l71Rl* null mutation. Since there are four genes located at the *l71Rl* locus, it is not clear how other three genes contribute to the *l71Rl* phenotype. It is possible that other candidate genes other than *Cyfip1* in the region or combination of more than one gene contribute to the phenotype of *l71Rl*. Future experiments could be considered of studying how the different combinations of four genes affect the mouse embryonic development. In addition, *Cyfip* has only one member in worm and fly, but it has two homologs in mice, *Cyfip1* and *Cyfip2*, with 88% identity at amino acid sequence level (Schenck, Bardoni et al. 2001). No *Cyfip2* mutation has been reported in mice, thus, its function during the mouse embryo development remains to be studied. It is interesting to note that human *Cyfip2* can functionally replace the plant *Cyfip* gene (Basu, El-Assal Sel et al. 2004). Although this study indicates that the loss of *Cyfip1* function can not be compensated by *Cyfip2*, there is still a possibility that *Cyfip2* might have overlapping function with *Cyfip1*. Studying the function of *Cyfip2* in mouse embryonic development will be helpful of understanding the peri-implantation failure.

Cyfip is one of the downstream effectors of Rac1 (Kobayashi, Kuroda et al. 1998), and it interacts directly with Rac1 and then binds to the other components of the WAVE2 protein complex to reorganize the actin network in the leading edge of the lamellipodia (Steffen, Rottner et al. 2004). Cyfip1-Rac1 protein complex is essential for membrane ruffling and other numerous cell processes, such as cell morphogenesis and cell migration. *Rac1* is expressed ubiquitously in the mouse embryo (Sugihara, Nakatsuji et al. 1998),

and is known to regulate the actin polymerization of the cytoskeleton in lamellipodia. Null mutation of *Rac1* results in failure of mouse embryo gastrulation (Sugihara, Nakatsuji et al. 1998), which is required for formation of all three germ layers during the gastrulation. Our data showed that *Cyfip1* was required for the neuronal morphogenesis during the mouse embryo development, therefore neuromorphogenesis likely relies on *Cyfip1*-Rac1 interaction and the related signal transduction pathways (Hall 1998). Biochemistry studies indicate that Cyfip1 is a specific target of Rac1 and the N-terminal of 1-407 amino acids of the Cyfip1 is responsible for the interaction with Rac1 (Kobayashi, Kuroda et al. 1998). Cyfip1 may be very important for the Rac1 functioning in the neuromorphogenesis.

Furthermore, the human ortholog Cyfip1 interacts with Fmr1, an RNA-binding protein associated with a messenger ribonucleoprotein (mRNP) complex and involved in local RNA translation in neural cell dendrites and dendritic spine maturation(Schenck, Bardoni et al. 2001). *Fmr1* null mutation in mice is viable with macroorchidism and behavior abnormality (Norton 1994). Both null mutations of *Rac1* and *Fmr1*, which are known to interact directly with *Cyfip1*, show different phenotypes to the *Cyfip1* mutations presented in this study; however these genes are all related to the neuron development. One hypothesis is that Cyfip1 regulates the neuronal development through protein-protein interaction with Rac1 and Fmr1 at different stage of mouse development. One experimental approach to study the role of Cyfip1 in the neuronal development could use P19 embryonic carcinoma cell line, which has been widely used as a neuronal development model (Mcburney and Rogers, 1982). The defective of Cyfip1 protein

leading to embryonic lethal has provided us an opportunity to understand the molecular mechanisms of neuron development.

REFERENCES

Alberman, E. D. and M. R. Creasy (1977). "Frequency of chromosomal abnormalities in miscarriages and perinatal deaths." J Med Genet 14(5): 313-5.

Amos-Landgraf, J. M., Y. Ji, et al. (1999). "Chromosome breakage in the Prader-Willi and Angelman syndromes involves recombination between large, transcribed repeats at proximal and distal breakpoints." Am J Hum Genet 65(2): 370-86.

Bard, J. B. L., Kaufman, M. H., Dubreuil, C., Brune, R.M., Burger, A., Baldock, R. A., Davidson, D. R. (1998). "An internet-accessible database of mouse developmental anatomy based on a systematic nomenclature." Mechanisms of Development.

Bardoni, B., A. Schenck, et al. (2001). "The Fragile X mental retardation protein." Brain Res Bull 56(3-4): 375-82.

Basu, D., D. El-Assal Sel, et al. (2004). "Interchangeable functions of Arabidopsis PIROGI and the human WAVE complex subunit SRA1 during leaf epidermal development." Development 131(17): 4345-55.

Blagg, S. L., M. Stewart, et al. (2003). "PIR121 regulates pseudopod dynamics and SCAR activity in Dictyostelium." Curr Biol 13(17): 1480-7.

Brannan, C. I., M. A. Bedell, et al. (1992). "Developmental abnormalities in Steel17H mice result from a splicing defect in the steel factor cytoplasmic tail." Genes Dev 6(10): 1832-42.

Chai, J. H., D. P. Locke, et al. (2003). "Identification of four highly conserved genes between breakpoint hotspots BP1 and BP2 of the Prader-Willi/Angelman syndromes deletion region that have undergone evolutionary transposition mediated by flanking duplicons." Am J Hum Genet 73(4): 898-925.

Chao, H. H., S. E. Mentzer, et al. (2003). "Overlapping deletions define novel embryonic lethal loci in the mouse t complex." Genesis 35(2): 133-42.

Culiat, C. T., L. Stubbs, et al. (1993). "Concordance between isolated cleft palate in mice and alterations within a region including the gene encoding the beta 3 subunit of the type A gamma-aminobutyric acid receptor." Proc Natl Acad Sci U S A 90(11): 5105-9.

Culiat, C. T., L. J. Stubbs, et al. (1994). "Phenotypic consequences of deletion of the gamma 3, alpha 5, or beta 3 subunit of the type A gamma-aminobutyric acid receptor in mice." Proc Natl Acad Sci U S A 91(7): 2815-8.

Ding, J., L. Yang, et al. (1998). "Cripto is required for correct orientation of the anterior-posterior axis in the mouse embryo." Nature 395(6703): 702-7.

Dockendorff, T. C., H. S. Su, et al. (2002). "Drosophila lacking dfmr1 activity show defects in circadian output and fail to maintain courtship interest." Neuron 34(6): 973-84.

Downes, K. M. a. D., T. (1993). "Staging of gastrulating mouse embryos by morphological landmarks in the dissecting microscope." Development 118: 1255-1266.

Eden, S., R. Rohatgi, et al. (2002). "Mechanism of regulation of WAVE1-induced actin nucleation by Rac1 and Nck." Nature 418(6899): 790-3.

Eicher, E. M. (1970). "The Position of ru-2 and qv with Respect to the FLECKED Translocation in the Mouse." Genetics 64(3-4): 495-510.

Fossett, N. G., P. Arbour-Reily, et al. (1990). "Analysis of ENU-induced mutations at the Adh locus in Drosophila melanogaster." Mutat Res 231(1): 73-85.

Gardner, J. M., Y. Nakatsu, et al. (1992). "The mouse pink-eyed dilution gene: association with human Prader-Willi and Angelman syndromes." Science 257(5073): 1121-4.

Goddijn, M. and N. J. Leschot (2000). "Genetic aspects of miscarriage." Baillieres Best Pract Res Clin Obstet Gynaecol 14(5): 855-65.

Hakeda-Suzuki, S., J. Ng, et al. (2002). "Rac function and regulation during Drosophila development." Nature 416(6879): 438-42.

Hall, A. (1998). "Rho GTPases and the actin cytoskeleton." Science 279(5350): 509-14.

Higgs, H. N. and T. D. Pollard (1999). "Regulation of actin polymerization by Arp2/3 complex and WASp/Scar proteins." J Biol Chem 274(46): 32531-4.

Hogan, B., Beddington, R., Costantini, F., and Lacy, E. (1994). "Manipulating the mouse embryo 2nd edition." Cold Spring Harbor laboratory press.

Inatani, M., F. Irie, et al. (2003). "Mammalian brain morphogenesis and midline axon guidance require heparan sulfate." Science 302(5647): 1044-6.

Ji, Y., M. J. Walkowicz, et al. (1999). "The ancestral gene for transcribed, low-copy repeats in the Prader-Willi/Angelman region encodes a large protein implicated in protein trafficking, which is deficient in mice with neuromuscular and spermiogenic abnormalities." Hum Mol Genet 8(3): 533-42.

Johnson, D. K., L. J. Stubbs, et al. (1995). "Molecular analysis of 36 mutations at the mouse pink-eyed dilution (p) locus." Genetics 141(4): 1563-71.

Kaufman, T. a. (1989). "The house mouse: Atlas of Embryonic Development."

Kaufmann, N., Z. P. Wills, et al. (1998). "Drosophila Rac1 controls motor axon guidance." Development 125(3): 453-61.

Kimura, C., K. Yoshinaga, et al. (2000). "Visceral endoderm mediates forebrain development by suppressing posteriorizing signals." Dev Biol 225(2): 304-21.

Knoll, J. H., R. D. Nicholls, et al. (1990). "Angelman syndrome: three molecular classes identified with chromosome 15q11q13-specific DNA markers." Am J Hum Genet 47(1): 149-55.

Kobayashi, K., S. Kuroda, et al. (1998). "p140Sra-1 (specifically Rac1-associated protein) is a novel specific target for Rac1 small GTPase." J Biol Chem 273(1): 291-5.

Koster, F., B. Schinke, et al. (1998). "Identification of shyc, a novel gene expressed in the murine developing and adult nervous system." Neurosci Lett 252(1): 69-71.

Laggerbauer, B., D. Ostareck, et al. (2001). "Evidence that fragile X mental retardation protein is a negative regulator of translation." Hum Mol Genet 10(4): 329-38.

Lee, S. T., R. D. Nicholls, et al. (1994). "Mutations of the P gene in oculocutaneous albinism, ocular albinism, and Prader-Willi syndrome plus albinism." N Engl J Med 330(8): 529-34.

Li, Z., Y. Zhang, et al. (2001). "The fragile X mental retardation protein inhibits translation via interacting with mRNA." Nucleic Acids Res 29(11): 2276-83.

Machesky, L. M. and R. H. Insall (1998). "Scar1 and the related Wiskott-Aldrich syndrome protein, WASP, regulate the actin cytoskeleton through the Arp2/3 complex." Curr Biol 8(25): 1347-56.

Machesky, L. M., R. D. Mullins, et al. (1999). "Scar, a WASp-related protein, activates nucleation of actin filaments by the Arp2/3 complex." Proc Natl Acad Sci U S A 96(7): 3739-44.

Miki, H., S. Suetsugu, et al. (1998). "WAVE, a novel WASP-family protein involved in actin reorganization induced by Rac." Embo J 17(23): 6932-41.

Morales, J., P. R. Hiesinger, et al. (2002). "Drosophila fragile X protein, DFXR, regulates neuronal morphology and function in the brain." Neuron 34(6): 961-72.

Murphy, S. M., A. M. Preble, et al. (2001). "GCP5 and GCP6: two new members of the human gamma-tubulin complex." Mol Biol Cell 12(11): 3340-52.

Ng, J., T. Nardine, et al. (2002). "Rac GTPases control axon growth, guidance and branching." Nature 416(6879): 442-7.

Nicholls, R. D., W. Gottlieb, et al. (1993). "Evaluation of potential models for imprinted and nonimprinted components of human chromosome 15q11-q13 syndromes by fine-structure homology mapping in the mouse." Proc Natl Acad Sci U S A 90(5): 2050-4.

Nicholls, R. D. and J. L. Knepper (2001). "Genome organization, function, and imprinting in Prader-Willi and Angelman syndromes." Annu Rev Genomics Hum Genet 2: 153-75.

Norton, P. A. (1994). "Alternative pre-mRNA splicing: factors involved in splice site selection." J Cell Sci 107 (Pt 1): 1-7.

Oegema, K., C. Wiese, et al. (1999). "Characterization of two related Drosophila gamma-tubulin complexes that differ in their ability to nucleate microtubules." J Cell Biol 144(4): 721-33.

Pollard, T. D. and G. G. Borisy (2003). "Cellular motility driven by assembly and disassembly of actin filaments." Cell 112(4): 453-65.

Popp, R. A., E. G. Bailiff, et al. (1983). "Analysis of a mouse alpha-globin gene mutation induced by ethylnitrosourea." Genetics 105(1): 157-67.

Rainier, S., J. H. Chai, et al. (2003). "NIPA1 gene mutations cause autosomal dominant hereditary spastic paraplegia (SPG6)." Am J Hum Genet 73(4): 967-71.

Rhinn, M., A. Dierich, et al. (1998). "Sequential roles for Otx2 in visceral endoderm and neuroectoderm for forebrain and midbrain induction and specification." Development 125(5): 845-56.

Ridley, A. J. (2001). "Rho family proteins: coordinating cell responses." Trends Cell Biol 11(12): 471-7.

Rinchik, E. M., S. J. Bultman, et al. (1993). "A gene for the mouse pink-eyed dilution locus and for human type II oculocutaneous albinism." Nature 361(6407): 72-6.

Rinchik, E. M., D. A. Carpenter, et al. (1995). "Pleiotropy in microdeletion syndromes: neurologic and spermatogenic abnormalities in mice homozygous for the p6H deletion are likely due to dysfunction of a single gene." Proc Natl Acad Sci U S A 92(14): 6394-8.

Rinchik, E. M., D. A. Carpenter, et al. (2002). "Functional annotation of mammalian genomic DNA sequence by chemical mutagenesis: a fine-structure genetic

mutation map of a 1- to 2-cM segment of mouse chromosome 7 corresponding to human chromosome 11p14-p15." Proc Natl Acad Sci U S A 99(2): 844-9.

Rugh, R. (1994). "The mouse: its reproduction and development." Oxford university press.

Russell, L. B., C. S. Montgomery, et al. (1995). "Complementation analyses for 45 mutations encompassing the pink-eyed dilution (p) locus of the mouse." Genetics 141(4): 1547-62.

Russell, W. L. (1951). "X-ray induced mutations in mice." Cold Spring Harbor Symp. Quant. Biology 16: 327-336.

Russell, W. L. (1989). "Reminiscences of a mouse specific-locus test addict." Environ Mol Mutagen 14 Suppl 16: 16-22.

Schaeffer, C., B. Bardoni, et al. (2001). "The fragile X mental retardation protein binds specifically to its mRNA via a purine quartet motif." Embo J 20(17): 4803-13.

Schenck, A., B. Bardoni, et al. (2003). "CYFIP/Sra-1 controls neuronal connectivity in Drosophila and links the Rac1 GTPase pathway to the fragile X protein." Neuron 38(6): 887-98.

Schenck, A., B. Bardoni, et al. (2001). "A highly conserved protein family interacting with the fragile X mental retardation protein (FMRP) and displaying selective interactions with FMRP-related proteins FXR1P and FXR2P." Proc Natl Acad Sci U S A 98(15): 8844-9.

Schenck, A., V. Van de Bor, et al. (2002). "Novel features of dFMR1, the Drosophila orthologue of the fragile X mental retardation protein." Neurobiol Dis 11(1): 53-63.

Siomi, M. C., H. Siomi, et al. (1995). "FXR1, an autosomal homolog of the fragile X mental retardation gene." Embo J 14(11): 2401-8.

Siomi, M. C., Y. Zhang, et al. (1996). "Specific sequences in the fragile X syndrome protein FMR1 and the FXR proteins mediate their binding to 60S ribosomal subunits and the interactions among them." Mol Cell Biol 16(7): 3825-32.

Soto, M. C., H. Qadota, et al. (2002). "The GEX-2 and GEX-3 proteins are required for tissue morphogenesis and cell migrations in C. elegans." Genes Dev 16(5): 620-32.

Spritz, R. A. (1994). "Molecular genetics of oculocutaneous albinism." Hum Mol Genet 3 Spec No: 1469-75.

Steffen, A., K. Rottner, et al. (2004). "Sra-1 and Nap1 link Rac to actin assembly driving lamellipodia formation." Embo J 23(4): 749-59.

Sugihara, K., N. Nakatsuji, et al. (1998). "Rac1 is required for the formation of three germ layers during gastrulation." Oncogene 17(26): 3427-33.

Thomas, P. and R. Beddington (1996). "Anterior primitive endoderm may be responsible for patterning the anterior neural plate in the mouse embryo." Curr Biol 6(11): 1487-96.

Walkowicz, M., Y. Ji, et al. (1999). "Molecular characterization of radiation- and chemically induced mutations associated with neuromuscular tremors, runting, juvenile lethality, and sperm defects in jdf2 mice." Mamm Genome 10(9): 870-8.

Wan, L., T. C. Dockendorff, et al. (2000). "Characterization of dFMR1, a Drosophila melanogaster homolog of the fragile X mental retardation protein." Mol Cell Biol 20(22): 8536-47.

Wienholds, E., F. van Eeden, et al. (2003). "Efficient target-selected mutagenesis in zebrafish." Genome Res 13(12): 2700-7.

Wu, M., E. M. Rinchik, et al. (2000). "An integrated deletion and physical map encompassing l71Rl, a chromosome 7 locus required for peri-implantation survival in the mouse." Genomics 67(2): 228-31.

Zdarsky, E., J. Favor, et al. (1990). "The molecular basis of brown, an old mouse mutation, and of an induced revertant to wild type." Genetics 126(2): 443-9.

Zhang, Y. Q., A. M. Bailey, et al. (2001). "Drosophila fragile X-related gene regulates the MAP1B homolog Futsch to control synaptic structure and function." Cell 107(5): 591-603.

Vita

Ling Li was born December 10, 1973, in Hami, Xinjiang Province, P. R. China. After graduating from Nanjing Railway Medical College P. R. China in 1997, Ling Li worked as a surgical resident in Xi'an Railway Central Hospital for over 2 years. She also worked as an instructor in Xi'an Xiandai Professional Medical College during that time. Ling Li came to the United States to join her husband in 2000 and started her graduate study in the graduate school of Genome Science and Technology, University of Tennessee – Oak Ridge National Laboratory, Knoxville in fall 2001. Ling Li is interested in medical related research.